6 Turbulence Closure Techniques

At first glance, the large number of equations developed in Chapters 3-5 would suggest that we have a fairly complete description of turbulent flow. Unfortunately, a closer examination reveals that there are a large number of unknowns remaining in those equations. These unknowns must be dealt with in order end up with a useful description of turbulence that can be applied to real situations. In this Chapter, the unknowns are identified, and methods to parameterize them are reviewed. Simulation techniques such as large-eddy simulation are discussed in Chapter 10.

6.1 The Closure Problem

As will be demonstrated below, ***the number of unknowns in the set of equations for turbulent flow is larger than the number of equations.*** A variable is considered to be unknown if one doesn't have a prognostic or diagnostic equation defining it. When equations are included for these unknowns (changing them to known variables), one discovers even more new unknowns. Thus, for any finite set of those equations the description of turbulence is not ***closed.*** Alternately, the total statistical description of turbulence requires an infinite set of equations. This unfortunate conclusion is called the ***closure problem.*** It was first recognized in 1924 by Keller and Friedmann, and was associated with the non-linear characteristic of turbulence. It has remained one of the unsolved problems of classical physics.

To demonstrate the closure problem, recall from equations 3.5.3 in Chapter 3 that the forecast equation for a mean variable such as potential temperature has at least one turbulence term in it, such as $\partial(\overline{u_j'\theta'})/\partial x_j$. A quantity like $\overline{u_j'\theta'}$ is called a ***double correlation***, or a ***second statistical moment***. To eliminate this as an unknown we derived a forecast equation for it in Chapter 4 (equation 4.4.3). Unfortunately, this equation contained additional ***triple correlation (third moment)*** terms such as $\overline{\theta' u_i' u_j'}$. As you might expect, if we were to write an equation for this third moment, it would contain a fourth-moment quantity.

The matter is even worse than highlighted above, because $\overline{\theta' u_i' u_j'}$ really represents 9 terms, one for each value of i and j. Of these 9 terms, 6 remain as unknowns because of symmetries in the tensor matrix (e.g., $\overline{\theta' u_1' u_2'} = \overline{\theta' u_2' u_1'}$). Similar problems occur for the turbulence equations for momentum, as is shown in Table 6-1. There is an easy way to anticipate which unknowns remain at any level of closure after symmetries are considered, as is shown in Table 6-2 for momentum correlations. In the full equations of motion there are additional unknowns such as pressure correlations and terms involving viscosity.

Table 6-1. Simplified example showing a tally of equations and unknowns for various statistical moments of momentum, demonstrating the closure problem for turbulent flow. The full set of equations includes even more unknowns.

Prognostic Eq. for:	Moment	Equation	Number of Eqs.	Number of Unknowns
$\overline{U_i}$	First	$\frac{\partial \overline{U_i}}{\partial t} = \ldots - \frac{\partial \overline{u_i' u_j'}}{\partial x_j}$	3	6
$\overline{u_i' u_j'}$	Second	$\frac{\partial \overline{u_i' u_j'}}{\partial t} = \ldots - \frac{\partial \overline{u_i' u_j' u_k'}}{\partial x_k}$	6	10
$\overline{u_i' u_j' u_k'}$	Third	$\frac{\partial \overline{u_i' u_j' u_k'}}{\partial t} = \ldots - \frac{\partial \overline{u_i' u_j' u_k' u_m'}}{\partial x_m}$	10	15

Table 6-2. Correlation triangles indicating the unknowns for various levels of turbulence closure, for the momentum equations only. Notice the pattern in these triangles, with the u, v, and w statistics at their respective vertices, and the cross correlations in between.

Order of Closure	Correlation Triangle of Unknowns
Zero	$\overline{U}$ $\overline{V}$ $\overline{W}$
First	$\overline{u'^2}$ $\overline{u'v'}$ $\overline{u'w'}$ $\overline{v'^2}$ $\overline{v'w'}$ $\overline{w'^2}$
Second	$\overline{u'^3}$ $\overline{u'^2v'}$ $\overline{u'^2w'}$ $\overline{u'v'^2}$ $\overline{u'v'w'}$ $\overline{u'w'^2}$ $\overline{v'^3}$ $\overline{v'^2w'}$ $\overline{v'w'^2}$ $\overline{w'^3}$

To make the mathematical/statistical description of turbulence tractable, one approach is to use only a finite number of equations, and then approximate the remaining unknowns in terms of known quantities. Such ***closure approximations*** or ***closure assumptions*** are named by the highest order prognostic equations that are retained. Using the equations in Table 6-1 as an example, for ***first-order closure*** the first equation is retained and the second moments are approximated. Similarly, ***second-order closure*** retains the first two equations, and approximates terms involving third moments.

Some closure assumptions utilize only a portion of the equations available within a particular moment category. For example, if equations for the turbulence kinetic energy

and temperature and moisture variance are used along with the first-moment equations of Table 6-1, the result can be classified as ***one-and-a-half order closure***. It clearly would not be full second-order closure because not all of the prognostic equations for the second moments (i.e., for the fluxes) are retained, yet it is higher order than first-order closure. One can similarly define ***zero-order closure*** and ***half-order closure*** methods.

Two major schools of thought of turbulence closure have appeared in the literature: ***local*** and ***nonlocal*** closure. Neither local nor nonlocal methods are exact, but both appear to work well for the physical situations for which the parameterizations are designed.

For ***local closure***, an unknown quantity at any point in space is parameterized by values and/or gradients of known quantities at the ***same*** point. Local closure thus assumes that turbulence is analogous to molecular diffusion. The Donaldson example in the next section demonstrates a local second-order closure. In the meteorological literature, local closure has been used at all orders up through third order.

For ***nonlocal closure***, the unknown quantity at one point is parameterized by values of known quantities at ***many points*** in space. This assumes that turbulence is a superposition of eddies, each of which transports fluid like an advection process. Nonlocal methods have been used mostly with first-order closure. Table 6-3 summarizes the myriad of closure methods which have often appeared in the meteorological literature. Generally, the higher-order local closures and the nonlocal closures yield more accurate solutions than lower order, but they do so at added expense and complexity.

Table 6-3. Classification of closure techniques that have been frequently reported in the literature. Bulk and similarity methods are discussed in more detail in Chapters 9, 11 and 12.

Order	Local	Nonlocal	Other (bulk or similarity methods)
Zero			X
Half	X	X	X
First	X	X	
One-and-a-half	X		
Second	X		
Third	X		

6.2 Parameterization Rules

Regardless of which order closure is used, there are ***unknown*** turbulence terms which must be parameterized as a function of ***known*** quantities and ***parameters***. A ***known*** quantity is any quantity for which a prognostic or diagnostic equation is retained. Using the equations in Table 6-1 for example, if we decide to use second-order closure,

the unknown quantity $\overline{u_i'u_j'u_k'}$ can be parameterized as a function of $\overline{U_i}$ and $\overline{u_i'u_j'}$, because we have prognostic equations for these quantities. One must remember that the equations in Table 6-1 are only a subset of the full set of equations, therefore second-order closure can also employ other known first and second moments such as $\overline{\theta}$, $\partial\overline{\theta}/\partial z$, or $\overline{w'q'}$ in the parameterization. A ***parameter*** is usually a constant, the value of which is determined empirically. For example, the parameter can be a separate term, a multiplicative constant, or the value of a power or exponent.

By definition, a ***parameterization*** is an approximation to nature. In other words, we are replacing the true (natural) equation describing a value with some artificially constructed approximation. Sometimes parameterizations are employed because the true physics has yet to be discovered. Other times, the known physics are too complicated to use for a particular application, given cost or computer limitations. Parameterization will rarely be perfect. The hope is that it will be adequate.

Parameterization involves human interpretation and creativity, which means that different investigators can propose different parameterizations for the same unknown. In fact, Donaldson (1973) noted that "there are more models for closure of the equations of motion at the second-order correlation level than there are principal investigators working on the problem". Although there is likely to be an infinite set of possible parameterizations for any quantity, all acceptable parameterizations must follow certain common-sense rules.

Most importantly,the parameterization for an unknown quantity should be physically reasonable. In addition, the parameterization must:

- have the same dimensions as the unknown.
- have the same tensor properties.
- have the same symmetries.
- be invariant under an arbitrary transformation of coordinate systems.
- be invariant under a Galilean (i.e., inertial or Newtonian) transformation.
- satisfy the same budget equations and constraints.

These rules apply to all orders of closure.

As an example, Donaldson (1973) has proposed that the ***unknown*** $\overline{u_i'u_j'u_k'}$ be parameterized by:

$$-\Lambda \bar{e}^{1/2}\left[\frac{\partial(\overline{u_j'u_k'})}{\partial x_i}+\frac{\partial(\overline{u_i'u_k'})}{\partial x_j}+\frac{\partial(\overline{u_i'u_j'})}{\partial x_k}\right]$$

where Λ is a ***parameter*** having the dimension of length (m), and the ***knowns*** are $\bar{e}$ (turbulence kinetic energy per unit mass, m^2s^{-2}) and $\overline{u_i'u_j'}$ (momentum flux, m^2s^{-2}).

This parameterization has the same dimensions (m^3s^{-3}) and the same tensor properties (unsummed i, j & k) as the original unknown. The symmetry of the original unknown is such that the order of the indices i, j, k is not significant. The same symmetry is achieved in the parameterization by having the sum of the three terms in square brackets. If only one term had been used instead of the sum, then a change in the order of the indices would have produced a different numerical result (because $\partial\,\overline{u'v'}/\partial z$ is not necessarily equal to $\partial\overline{u'w'}/\partial y$). Since the gradient of the momentum flux is taken in all three Cartesian directions in the square brackets, any rotation or displacement of the coordinate system will not change the result. Also, movement of the coordinate system at constant velocity c_i (a Galilean transformation) does not change the parameterization, as can be seen by setting $x_i = X_i + c_i\,t$.

The final rule is difficult to demonstrate here without a long explanation of all the constraints on the system, but as a sample we can look at one constraint. The original unknown appears in budget equation (4.4.1b) as $\partial\overline{u_i'u_j'u_k'}/\partial x_j$, which represents the turbulent transport of $u_i'u_k'$. When the vertical component of this term ($\partial\overline{u_i'u_j'u_k'}/\partial z$) is integrated over the depth of the boundary layer it should equal zero, because it represents a movement of existing momentum flux from one height to another. The momentum flux drained by this term from one location within the turbulent domain should be deposited in a different part, yielding no net increase or decrease in total integrated momentum flux. This budget constraint is indeed satisfied by the parameterization above, because each of the terms in square brackets becomes zero when integrated over the whole BL depth.

The remainder of this Chapter reviews some of the parameterizations that have been presented in the literature. This review is by no means comprehensive — it is meant only to demonstrate the various types of closure and their features. Regardless of the type of parameterization used, the result closes the equations of motion for turbulent flow and allows them to be solved for various forecasting, diagnostic, and other practical applications.

6.3 Local Closure — Zero and Half Order

6.3.1 Zero Order

Zero-order closure implies that no prognostic equations are retained, not even the equations for mean quantities. In other words, the mean wind, temperature, humidity, and other mean quantities are parameterized directly as a function of space and time. Obviously, this is neither local or nonlocal closure because it avoids the parameterization of turbulence altogether. For this reason, we will not dwell on zero-order closure here, but will come back to it later in Chapter 9 under the topic of ***similarity theory***.

6.3.2 Half-order

Half-order closure uses a subset of the first moment equations (3.5.3). A variation of this approach is called the ***bulk method***, where a profile shape for wind or temperature is assumed, but where the resulting wind or temperature curve can be shifted depending on the bulk-average background wind or temperature within the whole layer.

For example, a boundary-layer (bulk) average $\langle\overline{\theta}(t)\rangle$ is forecast using equations like (3.5.3), a profile shape $[\Delta\overline{\theta}(z)]$ is assumed, and then the final values of $\overline{\theta}(z,t)$ are found from $\overline{\theta}(z,t) = \langle\overline{\theta}(t)\rangle + \Delta\overline{\theta}(z)$. Such schemes are used for bulk or ***slab*** mixed-layer models with $\Delta\overline{\theta}(z) = 0$ at all heights (see Chapter 11); for cloud models with $\Delta\overline{\theta}(z)$ modeled as linear functions of height within separate cloud and subcloud layers (see Chapter 13); and for stable boundary layers with $\Delta\overline{\theta}(z)$ approximated with either linear, polynomial, or exponential profile shapes (see Chapter 12).

6.4 Local Closure — First Order

6.4.1 Definition

First-order closure retains the prognostic equations for only the zero-order mean variables such as wind, temperature, and humidity. As an example, consider the idealized scenario of a dry environment, horizontally homogeneous, with no subsidence. The geostrophic wind is assumed to be known as a prescribed boundary condition. The governing prognostic equations (3.5.3) for the zero-order variables then reduce to:

$$\frac{\partial\overline{U}}{\partial t} = f_c(\overline{V} - \overline{V_g}) - \frac{\partial(\overline{u'w'})}{\partial z} \qquad (6.4.1a)$$

$$\frac{\partial\overline{V}}{\partial t} = -f_c(\overline{U} - \overline{U_g}) - \frac{\partial(\overline{v'w'})}{\partial z}$$

$$\frac{\partial\overline{\theta}}{\partial t} = - \frac{\partial(\overline{w'\theta'})}{\partial z}$$

The unknowns in this set of equations are second moments: $\overline{u'w'}$, $\overline{v'w'}$ and $\overline{w'\theta'}$.

To close the above set of equations, we must parameterize the turbulent fluxes. If we let ξ be any variable, then one possible first-order closure approximation for flux $\overline{u_j'\xi'}$ is:

$$\overline{u_j'\xi'} = -K\frac{\partial\bar{\xi}}{\partial x_j} \qquad (6.4.1b)$$

where the parameter K is a scalar with units m^2s^{-1}. For positive K, (6.4.1b) implies that the flux $\overline{u_j'\xi'}$ flows down the local gradient of $\bar{\xi}$. This closure approximation is often called ***gradient transport theory*** or ***K-theory***. Although it is one of the simplest parameterizations, it frequently fails when larger-size eddies are present in the flow. Hence, we can catalog (6.4.1b) as a ***small-eddy closure*** technique.

K is known by a variety of names:

- eddy viscosity
- eddy diffusivity
- eddy-transfer coefficient
- turbulent-transfer coefficient
- gradient-transfer coefficient

because it relates the turbulent flux to the gradient of the associated mean variable. Sometimes, different K values are associated with different variables. A subscript "m" is used for momentum, resulting in K_m as the eddy viscosity. For heat and moisture, we will use K_H and K_E for the respective eddy diffusivities. There is some experimental evidence to suggest that for statically neutral conditions:

$$K_H = K_E = 1.35\,K_m \qquad (6.4.1c)$$

It is not clear why K_m should be smaller than the other K values. Perhaps pressure-correlation effects contaminated the measurements upon which (6.4.1c) was based.

6.4.2 Examples

Problem A: Given $K_H = 5\ m^2s^{-1}$ for turbulence within a background stable environment, where the local lapse rate is $\partial\bar{\theta}/\partial z = 0.01$ K/m. Find $\overline{w'\theta'}$, the kinematic heat flux.

Solution: Use $\overline{u_j'\xi'} = -K\,\partial\bar{\xi}/\partial x_j$. Let $\bar{\xi}$ represent $\bar{\theta}$, and set j =3. This gives:

$$\overline{w'\theta'} = -K_H\frac{\partial\bar{\theta}}{\partial z} = -\left(5\ m^2s^{-1}\right)\left(0.01\ K/m\right) = -0.05\ K\ m/s$$

Discussion: A negative heat flux would normally be expected in a statically stable environment, assuming only small eddies were present. In other words, in an environment with warm air above colder air, turbulence moves warm air down the gradient to cooler air, which in this case is a downward (or negative) flux.

Problem B: Suggest parameterizations to close the set of equations (6.4.1a).

Solution:

$$\overline{w'\theta'} = -K_H \frac{\partial \overline{\theta}}{\partial z}$$

$$\overline{u'w'} = -K_m \frac{\partial \overline{U}}{\partial z}$$

$$\overline{v'w'} = -K_m \frac{\partial \overline{V}}{\partial z}$$

Discussion: If these equations are plugged back into (6.4.1a), then there are 3 equations for the 3 unknowns $\overline{\theta}$, $\overline{U}$, and $\overline{V}$. This is a closed set which can be solved numerically if the K values are known. Although the assumption that K=constant is an easy assumption, it is the least realistic. It would be better to parameterize K as a function of the knowns: $\overline{\theta}$, $\overline{U}$, and $\overline{V}$, or of gradients of those knowns.

Problem C: Given $K_H = 5\ m^2 s^{-1}$ for turbulence within a background horizontally homogeneous environment, find $\overline{u'\theta'}$.

Solution:

$$\overline{u'\theta'} = -K_H \frac{\partial \overline{\theta}}{\partial x}$$

But $\partial\overline{\theta}/\partial x = 0$ for a horizontally homogeneous environment. Thus $\overline{u'\theta'} = 0$.

Discussion: It makes no difference whether K_H is positive, negative or exceptionally large. K-theory will always yield zero flux in a uniform environment, regardless of the true flux.

6.4.3 Analogy with Viscosity

As we saw in Section 2.9.3, the molecular stress τ_{mol} can be approximated by $\tau_{mol} = \rho\ \nu\ \partial\overline{U}/\partial z$ for a Newtonian fluid. By analogy, one might expect that the turbulent Reynold's stress can be also expressed in terms of the shear, with a corresponding change from molecular viscosity ν to eddy viscosity K_m, yielding: $\tau_{Reynolds} = \rho\ K_m\ \partial\overline{U}/\partial z$. Dividing this latter expression by ρ gives the kinematic form (6.4.1b). The product $\rho \cdot K_m$ is sometimes called the ***Austausch coefficient***.

Since turbulence is much more effective than viscosity at causing mixing, one would expect $K_m > \nu$. Values of K_m reported in the literature vary from 0.1 m^2s^{-1} to 2000 m^2s^{-1}, with typical values on the order of 1 to 10 m^2s^{-1}. Values of ν are much smaller, on the order of $1.5x10^{-5}$ m^2s^{-1}.

Magnitude is not the only difference between the molecular and eddy viscosities. A significant difference is that ν is a function of the fluid, while K_m is a function of the flow. Thus, while ν is uniquely determined by the chemical composition of the fluid and its state (temperature and pressure, etc.), K_m varies as the turbulence varies. Thus, one must parameterize K_m as a function of other variables such as z/L, Richardson number or the stability $\partial\overline{\theta}_v/\partial z$, as outlined in Section 6.3.2.4.

6.4.4 Mixing-Length Theory

The following development is patterned after the mixing-length arguments proposed by Prandtl in 1925. Assume that there is turbulence in a statically neutral environment, with a linear mean humidity gradient in the vertical as sketched in Fig 6.1a. If a turbulent eddy moves a parcel of air upward by amount z' towards some reference level Z during which there is no mixing nor other changes in the value of q within the parcel, then the humidity of that parcel will differ from the surrounding environment by amount q', where:

$$q' = -\left(\frac{\partial\overline{q}}{\partial z}\right) z' \qquad (6.4.4a)$$

If the background mean wind profile is also linear, then a similar expression can be written for u':

$$u' = -\left(\frac{\partial\overline{U}}{\partial z}\right) z' \qquad (6.4.4b)$$

In order for the parcel to move upward a distance z', it must have had some vertical velocity w'. If the nature of turbulence is such that w' is proportional to u', then we might expect that $w' = -c\,u'$ for the the wind shear sketched in Fig 6.1b (i.e., for $\partial\overline{U}/\partial z > 0$), and $w' = c\,u'$ for $\partial\overline{U}/\partial z < 0$, where c is a constant of proportionality. Substituting (6.4.4b) for u' in the above expression for w' yields

$$w' = c\left|\frac{\partial\overline{U}}{\partial z}\right| z' \qquad (6.4.4c)$$

where we find that the magnitude of the shear is important.

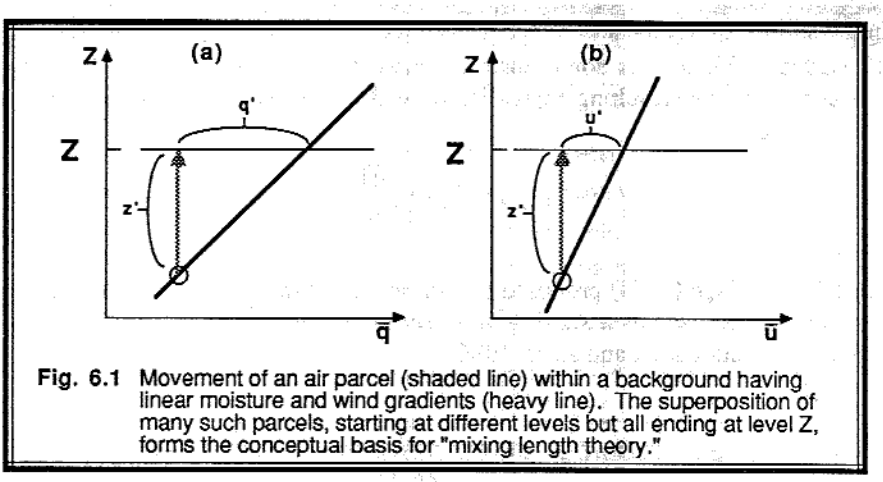

Fig. 6.1 Movement of an air parcel (shaded line) within a background having linear moisture and wind gradients (heavy line). The superposition of many such parcels, starting at different levels but all ending at level Z, forms the conceptual basis for "mixing length theory."

In Sections 2.6 and 2.7 it was shown that the kinematic eddy flux of moisture is $R = \overline{w'q'}$. Since we know q' from (6.4.4a) and w' from (6.4.4c), we need only multiply the two together, and then average over the spectrum of different size eddies z' to get the average flux R:

$$R = - c \overline{(z')^2} \left| \frac{\partial \bar{U}}{\partial z} \right| \cdot \left(\frac{\partial \bar{q}}{\partial z} \right) \qquad (6.4.4d)$$

We recognize $\overline{z'^2}$ as the variance of parcel displacement distance. The square root of it is a measure of the average distance a parcel moves in the mixing process that generated flux R. In this way, we can define a ***mixing length***, l, by $l^2 = c\,\overline{z'^2}$. Thus, the final expression for moisture flux is

$$R = - l^2 \left| \frac{\partial \bar{U}}{\partial z} \right| \cdot \left(\frac{\partial \bar{q}}{\partial z} \right) \qquad (6.4.4e)$$

This is directly analogous to K-theory if

$$K_E = l^2 \left| \frac{\partial \bar{U}}{\partial z} \right| \qquad (6.4.4f)$$

because that leaves us with $R = - K_E (\partial \bar{q}/\partial z)$. In fact, mixing-length theory tells us via (6.4.4f) that the magnitude of K_E should increase as the shear increases (i.e., a measure of the intensity of turbulence) and as the mixing length increases (i.e., a measure of the ability of turbulence to cause mixing).

In the surface layer, the size of the turbulent eddies is limited by the presence of the earth's surface. Thus, it is sometimes assumed that $l^2 = k^2z^2$, where k is the von Karman constant. The resulting expression for eddy viscosity in the surface layer is

$$K_E = k^2z^2 \left| \frac{\partial \overline{U}}{\partial z} \right| \qquad (6.4.4g)$$

For SBLs, Delage (1974) proposed the following parameterization for mixing length that has since been used as a starting point for other parameterizations (Estournel and Guedalia, 1987; and Lasser and Arya, 1986):

$$\frac{1}{l} = \frac{1}{kz} + \frac{1}{0.0004\, G\, f_c^{-1}} + \frac{\beta}{k L_L} \qquad (6.4.4h)$$

where L_L is a local Obukhov length (see Appendix A) based on local values of stress and heat flux above the surface, G is geostrophic wind speed, and β is an empirical constant.

Before leaving this section, we should examine the ***limitations*** of mixing-length theory. The relationship between w' and z' given by (6.4.4c) is only valid when turbulence is generated mechanically. Hence, mixing-length derivation is valid only for ***statically neutral situations***, even though K-theory has been applied to statically stable conditions. Also, linear gradients of wind and moisture were assumed in (6.4.4a & b). In the real atmosphere, gradients are approximately linear only over small distances (i.e., the first-order term of a Taylor's series expansion). Hence, we see that mixing-length theory is a ***small-eddy theory***.

6.4.5 Sample Parameterizations of K

The eddy viscosity is best not kept constant, as mentioned earlier, but should be parameterized as a function of the flow. The parameterizations for K should satisfy the following constraints:

- K = 0 where there is no turbulence.
- K = 0 at the ground (z=0).
- K increases as TKE increases.
- K varies with static stability (in fact, one might expect that a different value of K should be used in each of the coordinate directions for anisotropic turbulence).
- K is non-negative (if one uses the analogy with viscosity).

This latter constraint has occasionally been ignored. The normal concept of an eddy viscosity or a small-eddy theory is that a turbulent flux flows down the gradient. Such a ***down-gradient transport*** means heat flows from hot to cold, moisture flows from moist to dry, and so forth. Such down-gradient transport is associated with positive values for K, and is indeed consistent with the analogy with molecular viscosity.

Table 6-4. Examples of parameterizations for the eddy viscosity, K, in the boundary layer.

Neutral Surface Layer:	
$K = \text{constant}$	not the best parameterization
$K = u_*^2 T_o$	where u_* is the friction velocity
$K = U^2 T_o$	where T_o is a timescale
$K = k z u_*$	where k is von Karman's constant
$K = k^2 z^2 [(\partial\bar{U}/\partial z)^2 + (\partial\bar{V}/\partial z)^2]^{1/2}$	from mixing-length theory
$K = l^2 (\partial\bar{U}/\partial z)^2$	where $l = k(z+z_o)/\{1+[k(z+z_o)/\Lambda]\}$, Λ=length scale
Diabatic Surface Layer (generally, $K_{\text{statically unstable}} > K_{\text{neutral}} > K_{\text{statically stable}}$)	
$K = k z u_* / \phi_M (z/L)$	where ϕ_M a dimensionless shear (see appendix A), and L is the Obukhov length (appendix A)
$K = k^2 z^2 [(\partial\bar{U}/\partial z) + \{(g/\overline{\theta_v})\cdot\lvert\partial\overline{\theta_v}/\partial z\rvert\}^{1/2}]$	for statically unstable conditions
$K = k^2 z^2 [(\partial\bar{U}/\partial z) - (L_*/z)^{1/6}\{(15g/\overline{\theta_v})\cdot\lvert\partial\overline{\theta_v}/\partial z\rvert\}^{1/2}]$	for statically stable conditions, where $L_* = -\theta u_*^2/(15 k g \theta_*)$
Neutral or Stable Boundary Layer	
$K = \text{constant}$	see Ekman Spiral derivation in next subsection
$K = K(h) + [(h-z)/(h-z_{SL})]^2 \{K(z_{SL}) - K(h) + (z-z_{SL})[\partial K/\partial z\rvert_{z_{SL}} + 2(K(z_{SL})-K(h))/(h-z_{SL})]\}$	this is known as the O'Brien cubic polynomial approximation (O'Brien, 1970), see Fig 6-2, where z_{SL} represents the surface layer depth.
Unstable (Convective) Boundary Layer:	
$K = 1.1 [(R_c - Ri)/Ri]^2 \lvert\partial\bar{U}/\partial z\rvert$	for $\partial\overline{\theta_v}/\partial z > 0$ where $l = kz$ for $z < 200$ m and
$K = (1 - 18 Ri)^{-1/2} l^2 \lvert\partial\bar{U}/\partial z\rvert$	for $\partial\overline{\theta_v}/\partial z < 0$ $l = 70$ m for $z > 200$ m.
Numerical Model Approximation for Anelastic 3-D Flow:	
$K = (0.25\Delta)^2 \cdot \lvert 0.5 \Sigma_i \Sigma_j [\partial\bar{U}_i/\partial x_j + \partial\bar{U}_j/\partial x_i - (2/3)\delta_{ij}\Sigma_k(\partial\bar{U}_k/\partial x_k)]^2 \rvert^{1/2}$	where Δ=grid size

In the real atmosphere, however, there are occasions where transport appears to flow UP the gradient (i.e., ***counter-gradient***). As it turns out, this is physically explained by the fact that there are large eddies associated with rise of warm air parcels that transport heat from hot to cold, regardless of the local gradient of the background environment. Thus, in an attempt to make small-eddy K-theory work in large-eddy convective boundary layers, one must resort to negative values of K. Since this results in heat flowing from cold to hot, it is counter to our common-sense concept of diffusion. Thus, ***K-theory is not recommended for use in convective mixed layers.***

There has been no lack of creativity by investigators in designing parameterizations for K. Table 6-4 lists some of the parameterizations for K that have appeared in the literature (Bhumralkar, 1975), and Fig 6.2 show a typical variation of K with height in the boundary layer. Variations of K in the horizontal have also been suggested to explain phenomena such as mesoscale cellular convection (Ray, 1986).

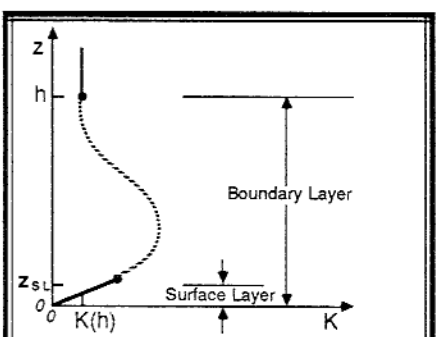

Fig. 6.2 Typical variation of eddy viscosity, K, with height in the boundary layer. After O'Brien (1970).

6.4.6 The Ekman Spiral in Atmospheres and Oceans

Even with first-order closure, the equations of motion (3.5.3) are often too difficult to solve analytically. However, for the special case of a steady state [$\partial\overline{(\ )}/\partial t=0$], horizontally homogeneous [$\partial\overline{(\ )}/\partial x = 0$, $\partial\overline{(\ )}/\partial y = 0$], statically neutral [$\partial\overline{\theta}_v/\partial z = 0$], barotropic atmosphere [$\overline{U}_g$ & $\overline{V}_g$ constant with height] with no subsidence [$\overline{W}=0$], the equations of motion can be reduced to:

$$\begin{cases} 0 = -f_c\left(\overline{V_g} - \overline{V}\right) - \dfrac{\partial\left(\overline{u'w'}\right)}{\partial z} \\ 0 = +f_c\left(\overline{U_g} - \overline{U}\right) - \dfrac{\partial\left(\overline{v'w'}\right)}{\partial z} \end{cases} \qquad (6.4.6a)$$

An analytic solution of these equations for the ocean was presented by Ekman in 1905, and was soon modified for the atmosphere.

Atmosphere: The following derivations are based on the approach of Businger (1982). Define the magnitude of the geostrophic wind, $\overline{G}$, by $\overline{G} = [\,\overline{U_g}^2 + \overline{V_g}^2\,]^{1/2}$. Pick an x-axis aligned with the geostrophic wind; thus, $\overline{V_g} = 0$ and $\overline{U_g} = \overline{G}$. Use first-order local closure K-theory, with constant K_m. Hence, $\overline{u'w'} = -K_m\,\partial\overline{U}/\partial z$ and $\overline{v'w'} = -K_m\,\partial\overline{V}/\partial z$. Inserting these into (6.4.6a) leaves the following set of coupled second-order differential equations:

$$\begin{cases} f_c\,\overline{V} = -K_m\dfrac{\partial^2\overline{U}}{\partial z^2} \\ f_c\left(\overline{U} - \overline{G}\right) = +K_m\dfrac{\partial^2\overline{V}}{\partial z^2} \end{cases} \qquad (6.4.6b)$$

The four boundary conditions are $\overline{U} = 0$ at $z = 0$, $\overline{V} = 0$ at $z = 0$, $\overline{U} \to \overline{G}$ as $z \to \infty$, and $\overline{V} = 0$ as $z \to \infty$. It is assumed that the winds become geostrophic away from the surface.

The solution to this set of equations for the atmosphere is

$$\begin{aligned} \overline{U} &= \overline{G}\left[1 - e^{-\gamma_E z}\cos\left(\gamma_E z\right)\right] \\ \overline{V} &= \overline{G}\left[e^{-\gamma_E z}\,\sin\left(\gamma_E z\right)\right] \end{aligned} \qquad (6.4.6c)$$

where $\gamma_E = [f_c/(2K_m)]^{1/2}$. The velocity vectors for this solution as a function of height are plotted in Fig 6.3a. The tip of the vectors trace out a spiral — hence the name ***Ekman Spiral.***

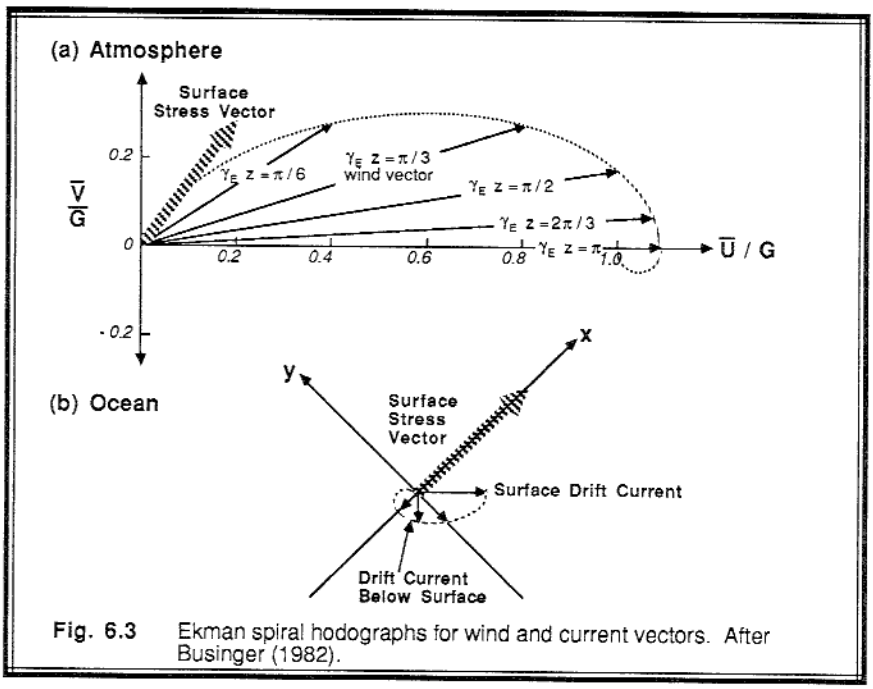

Fig. 6.3 Ekman spiral hodographs for wind and current vectors. After Businger (1982).

According to this solution, the surface wind vector is 45° to the left of the geostrophic wind vector in the Northern Hemisphere. Hence, the surface stress is also in this direction, because it is caused by the drag of the surface wind against the surface. Use u_*^2 as a measure of the surface stress magnitude, where $u_*^2 = [(\overline{u'w'})^2 + (\overline{v'w'})^2]^{1/2} = [(K_m \partial\overline{U}/\partial z)^2 + (K_m \partial\overline{V}/\partial z)^2]^{1/2}$ evaluated at z=0. Inserting (6.4.6c) into this expression yields:

$$u_*^2 = \overline{G}\left(K_m f_c\right)^{1/2} \tag{6.4.6d}$$

The wind speed is supergeostrophic at height $z = \pi/\gamma_E$, which is also the lowest height where the wind is parallel to geostrophic. Sometimes this height is used as an estimate of the ***depth of the neutral boundary layer.*** Hence, the ***Ekman layer depth***, h_E, is defined as $h_E = \pi/\gamma_E$. If K_m is assumed to equal $c \cdot k \cdot u_* \cdot h_E$, where c is a constant of proportionality equal to about 0.1, and k is the von Karman constant, then the Ekman layer depth for a neutral boundary layer becomes:

$$h_E = 2\,c\,k\,\pi^2\left(\frac{u_*}{f_c}\right) \tag{6.4.6e}$$

The major conclusion from the Ekman solution is that friction reduces the boundary layer wind speed below geostrophic, and causes it to cross the isobars from high towards low pressure. In a synoptic situation where the isobars are curved, such as a low or high pressure system, the ***cross-isobaric component of flow*** near the surface causes convergence or divergence, respectively. Hence, mass continuity requires that there be rising air in low pressure systems, and descending air in highs. The process of inducing vertical motions by boundary layer friction is called ***Ekman pumping***.

Ocean. The ocean drift current is driven by the wind stress at the surface, neglecting pressure gradients in the ocean. Hence, the equations of motion reduce to:

$$f_c \overline{V} = - K_m \frac{\partial^2 \overline{U}}{\partial z^2}$$

$$f_c \overline{U} = + K_m \frac{\partial^2 \overline{V}}{\partial z^2} \qquad (6.4.6f)$$

This time, let us choose a coordinate system with the x-axis aligned with the surface stress, and z positive up. Thus, the four boundary conditions become: $K_m \partial \overline{U}/\partial z = u_*^2$ at $z = 0$, $\partial \overline{V}/\partial z = 0$ at $z = 0$, $\overline{U} \to 0$ as $z \to -\infty$, and $\overline{V} \to 0$ as $z \to -\infty$. Thus, the current is assumed to go to zero deep in the ocean. In the equations above, K_m and u_* refer to their ocean values, where $\rho_{water} \cdot u_{*water}^2$ = surface stress = $\rho_{air} \cdot u_{*air}^2$.

The solution is:

$$\overline{U} = \left[\frac{u_*^2}{\left(K_m f_c \right)^{1/2}} \right] \left[e^{\gamma_E z} \cos\left(\gamma_E z - \frac{\pi}{4} \right) \right]$$

$$\overline{V} = \left[\frac{u_*^2}{\left(K_m f_c \right)^{1/2}} \right] \left[e^{\gamma_E z} \sin\left(\gamma_E z - \frac{\pi}{4} \right) \right] \qquad (6.4.6g)$$

where K_m and γ_E now apply to ocean values. This solution gives a surface current that is 45° to the right of the surface stress, making it parallel to the geostrophic wind in the atmosphere. Based on typical values of eddy viscosity in the air and ocean, the magnitude of the surface drift current is roughly G/30. Deeper in the ocean the current reduces in speed, and turns to the right as shown in Fig 6.3b. This causes horizontal convergence in the ocean under atmospheric regions of horizontal divergence, and vice versa. Hence, we expect ***downwelling*** water movement under synoptic high pressure systems, and ***upwelling*** under lows.

Discussion. Although the Ekman solution is analytic and has been around for a long time, the conditions under which it was derived rarely happen in nature in the atmosphere. At best, it gives an approximate quantitative solution for statically neutral boundary layers (i.e., mechanical turbulence production characteristic of strong winds, with no buoyancy effects). ***For convective mixed layers, the Ekman profile shape is not observed***, although it qualitatively agrees with the observed winds, which are subgeostrophic and cross-isobaric. ***Observed stable boundary layers can have supergeostrophic winds at low altitudes, making the Ekman solution even qualitatively incorrect.***

6.5 Local Closure — One-and-a-half Order

One-and-a-half-order closure retains the prognostic equations for the zero-order statistics such as mean wind, temperature, and humidity, and also retains equations for the variances of those variables. The TKE equation is usually used in place of the velocity variance equations. The following development is based on the work of Yamada & Mellor (1975).

As an example, consider the idealized scenario of a dry environment, horizontally homogeneous, with no subsidence. The governing prognostic equations are (3.5.3) for the zero-order variables, (4.3.3) for the temperature variance, and (5.1b) for TKE:

$$\frac{\partial \overline{U}}{\partial t} = f_c\left(\overline{V} - \overline{V}_g\right) - \frac{\partial \left(\overline{u'w'}\right)}{\partial z} \tag{6.5a}$$

$$\frac{\partial \overline{V}}{\partial t} = -f_c\left(\overline{U} - \overline{U}_g\right) - \frac{\partial \left(\overline{v'w'}\right)}{\partial z}$$

$$\frac{\partial \overline{\theta}}{\partial t} = - \frac{\partial \left(\overline{w'\theta'}\right)}{\partial z}$$

$$\frac{\partial \overline{e}}{\partial t} = - \overline{u'w'} \frac{\partial \overline{U}}{\partial z} - \overline{v'w'} \frac{\partial \overline{V}}{\partial z} + \left(\frac{g}{\overline{\theta}}\right) \overline{w'\theta'} - \frac{\partial \left[\overline{w'\left((p'/\rho) + e\right)}\right]}{\partial z} - \varepsilon$$

$$\frac{\partial \left(\overline{\theta'^2}\right)}{\partial t} = - 2\,\overline{w'\theta'} \frac{\partial \overline{\theta}}{\partial z} - \frac{\partial \left(\overline{w'\theta'^2}\right)}{\partial z} - 2\,\varepsilon_\theta - \varepsilon_R$$

The unknowns in this set of equations include second moments (fluxes): $\overline{u'w'}$, $\overline{v'w'}$, $\overline{w'\theta'}$, $\overline{w'p'}/\overline{\rho}$; third moments: $\overline{w'e}$, $\overline{w'\theta'^2}$; and dissipations: ε, ε_θ, and ε_R.

At first glance, the addition of the variance equations appears to have hurt us rather than helped us. With first-order closure we had the 3 unknown fluxes: $\overline{u'w'}$, $\overline{v'w'}$, $\overline{w'\theta'}$. The addition of the variance equations did not eliminate these fluxes as unknowns, and in fact added 6 more unknowns. So why did we do it?

The reason is that knowledge of the TKE and temperature variance gives us a measure of the intensity and effectiveness of turbulence. Hence, we can use this information within improved parameterizations for eddy diffusivity, $K_m(\bar{e}, \overline{\theta'^2})$. One suggested set of parameterizations for the unknowns is:

$$\overline{u'w'} = -K_m\left(\bar{e}, \overline{\theta'^2}\right)\frac{\partial \bar{U}}{\partial z} \tag{6.5b}$$

$$\overline{v'w'} = -K_m\left(\bar{e}, \overline{\theta'^2}\right)\frac{\partial \bar{V}}{\partial z}$$

$$\overline{w'\theta'} = -K_H\left(\bar{e}, \overline{\theta'^2}\right)\frac{\partial \bar{\theta}}{\partial z} - \gamma_c\left(\bar{e}, \overline{\theta'^2}\right)$$

$$\overline{w'\left[(p'/\bar{\rho}) + e\right]} = \left(\frac{5}{3}\right)\Lambda_4 e^{-1/2}\frac{\partial \bar{e}}{\partial z}$$

$$\overline{w'\theta'^2} = \Lambda_3 e^{-1/2}\frac{\partial \overline{\theta'^2}}{\partial z}$$

$$\varepsilon_R = 0 \qquad \varepsilon = \frac{\bar{e}^{3/2}}{\Lambda_1} \qquad \varepsilon_\theta = \frac{\bar{e}^{1/2}\,\overline{\theta'^2}}{\Lambda_2}$$

where the Λ factors are empirical length-scale parameters. These length scales are often chosen by trial and error, in an attempt to make the simulated flow field match observed laboratory or field cases. One problem with the closure of (6.5b) is that the length scales are rather arbitrary.

The expressions for K are too complex to reproduce here, but can approximately be represented by:

$$K = \Lambda\,\bar{e}^{1/2} \tag{6.5c}$$

where Λ represents one of the empirical length scales.

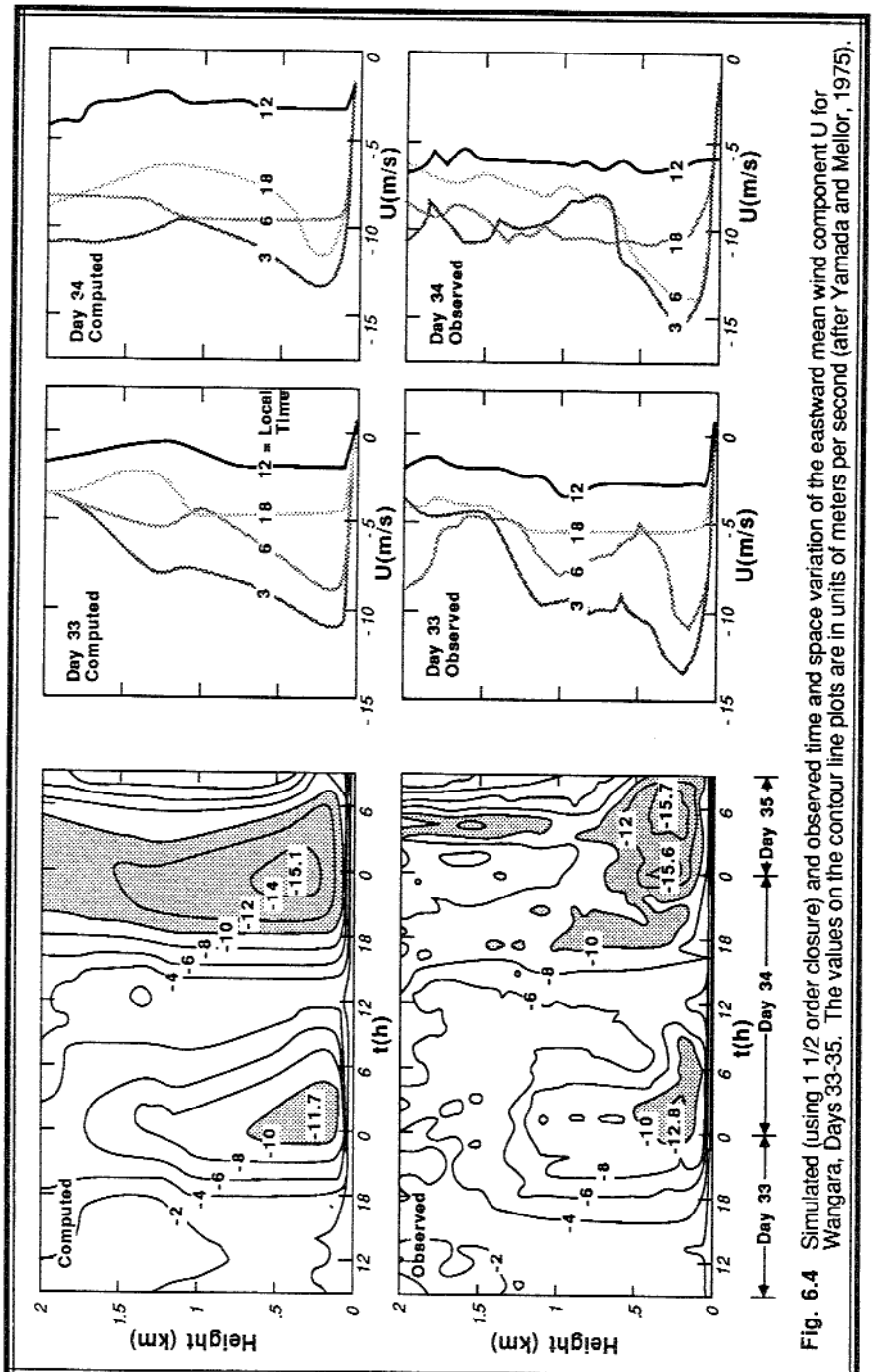

Fig. 6.4 Simulated (using 1 1/2 order closure) and observed time and space variation of the eastward mean wind component U for Wangara, Days 33-35. The values on the contour line plots are in units of meters per second (after Yamada and Mellor, 1975).

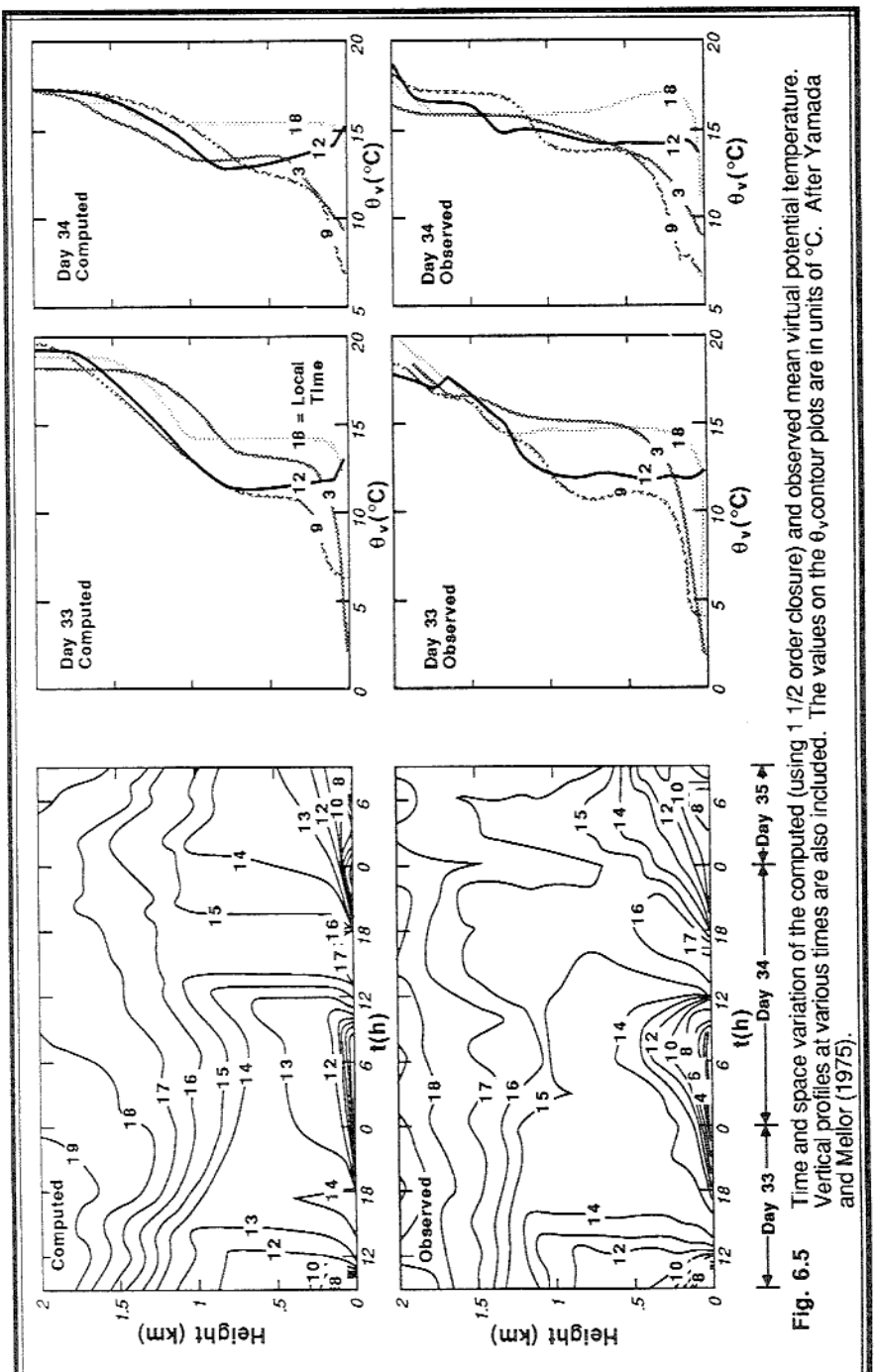

Fig. 6.5 Time and space variation of the computed (using 1 1/2 order closure) and observed mean virtual potential temperature. Vertical profiles at various times are also included. The values on the θ_v contour plots are in units of °C. After Yamada and Mellor (1975).

The second correlation terms are approximated as functions of gradients of mean values (e.g., the vertical flux of temperature, $\overline{w'\theta'}$, flows down the local vertical gradient of temperature $\partial\bar{\theta}/\partial z$). Similarly, the triple correlation terms are approximated as functions of gradients of second correlations (e.g., the vertical flux of temperature variance $\overline{w'\theta'^2}$ flows down the local vertical gradient of temperature variance $\partial\overline{\theta'^2}/\partial z$). The higher-order closure is thus very similar to the first-order closure — both depend on the local gradients and values of knowns.

The viscous dissipation terms of TKE and temperature variance are modeled as being proportional to their respective variables. For this reason, dissipation rates are sometimes used as a measure of the intensity of turbulence. More intense turbulence dissipates faster than weaker turbulence. The modeled dissipation rate has a timescale of $\Lambda/\bar{e}^{1/2}$. The γ_c parameter is added to the parameterization of $\overline{w'\theta'}$ to allow heat flux even when there is no mean gradient. This allows better representations of mixed layers. The pressure and turbulent transport terms assume that transport is down the mean TKE gradient.

The set of equations given by (6.5a & b) is too complex to solve analytically. Typically, these equations are approximated by their finite difference equivalents, and then solved numerically on a digital computer. Figs 6.4 through 6.6 shows a boundary-layer numerical simulation of a two day period from the Wangara field experiment. This simulation, produced by Yamada and Mellor using their one-and-a-half-order closure, not only shows the evolution of mean quantities such as wind (Fig 6.4) and virtual potential temperature (Fig 6.5), but it also shows the evolution of TKE (refer back to Fig 5.1) and temperature variance (Fig 6.6).

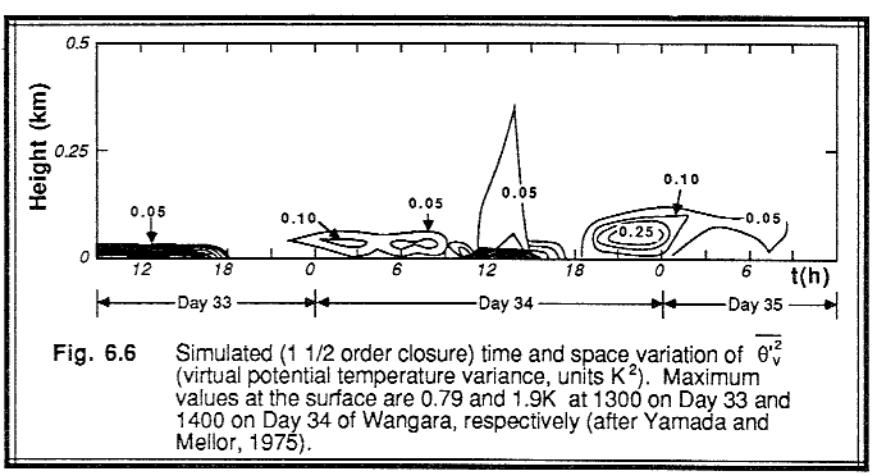

Fig. 6.6 Simulated (1 1/2 order closure) time and space variation of $\overline{\theta_v'^2}$ (virtual potential temperature variance, units K^2). Maximum values at the surface are 0.79 and 1.9K at 1300 on Day 33 and 1400 on Day 34 of Wangara, respectively (after Yamada and Mellor, 1975).

An alternative approach, called $\bar{e}$-ε ***closure*** (or ***k-ε closure*** in the engineering literature) avoids the Λ uncertainty by including a highly-parameterized prognostic equation for the dissipation rate in addition to the equation for TKE (Beljaars, et al., 1987; Kitada, 1987; Detering and Etling, 1985). The dissipation equation, which should be included with (6.5a), is sometimes written as:

$$\frac{\partial \varepsilon}{\partial t} = c_{\varepsilon 1} \frac{\varepsilon}{\bar{e}} \left[- \overline{u'w'} \frac{\partial \bar{U}}{\partial z} - \overline{v'w'} \frac{\partial \bar{V}}{\partial z} \right] + c_{\varepsilon 2} \frac{\varepsilon}{\bar{e}} \left(\frac{g}{\bar{\theta}} \right) \overline{w'\theta'} - \frac{\partial \overline{w'\varepsilon}}{\partial z} - c_{\varepsilon 3} \frac{\varepsilon^2}{\bar{e}} \qquad (6.5d)$$

where the parameters are $c_{\varepsilon 1} = 1.44$, $c_{\varepsilon 2} = 1.0$, and $c_{\varepsilon 3} = 1.92$.

The following additional closure assumption should also be added to (6.5b):

$$\overline{w'\varepsilon'} = - \frac{K}{c_{\varepsilon 4}} \frac{\partial \varepsilon}{\partial z} \qquad (6.5e)$$

where $c_{\varepsilon 4} = 1.3$. In place of (6.5c), the eddy diffusivity can now be parameterized as:

$$K = \frac{(c_{\varepsilon 5} \bar{e})^2}{\varepsilon} \qquad (6.5f)$$

where $c_{\varepsilon 5} = 0.3$. Similarly, the remaining length scales in (6.5b) are hopefully more accurate because they are a function of prognostic variables:

$$\Lambda = \frac{\bar{e}^{3/2}}{\varepsilon} \qquad (6.5g)$$

The k-ε version of one-and-a-half-order closure has been used to simulate boundary layer evolution, flow over changes in roughness and topography, and sea-breeze fronts.

By studying Figs 6.4 to 6.6, we can learn some of the advantages of higher-order closure. (1) The higher-order scheme creates nearly well-mixed layers during the daytime that increase in depth with time. (2) At night, there is evidence of nocturnal jet formation along with the development of a statically stable layer near the ground. (3) Turbulence intensity increases to large values during the day, but maintains smaller values at night in the nocturnal boundary layer. First-order closure, on the other hand, gives no information on turbulence intensity or temperature variance. Furthermore, it has difficulty with well mixed layers that have zero gradients of mean variables. However, the benefits of higher-order closure do not come cheaply; they are gained at the expense of increased computer time and cost compared to first-order closure.

6.6 Local Closure — Second Order

The development of ***higher-order closure*** (usually meaning anything higher than first-order closure) was closely tied to the evolution of digital computer power. Although the use of higher-moment equations for turbulence forecasting was suggested in the early 1940's, the large number of unknown variables remained a stumbling block. Then, around 1950, Rotta and Chou and others suggested parameterizations for some of the unknowns. By the late 1960's, computer power improved to the point where second-order closure forecasts for clear air turbulence and shear flows were first made. In the early 1970's, the United States Environmental Protection Agency began funding some second-order closure pollution dispersion models, and by the mid 1970's a number of investigators were using such models. In fact, second-order closure appears to have started before one-and-a-half-order closure. In the late 1970's, some third-order closure models also started to appear in the literature, with many more third-order simulations published in the 1980's.

The set of second-order turbulence equations includes not only those from one-and-a-half-order, but it includes second moment terms as well (Wichmann and Schaller, 1986). Using the same idealized example as above, consider a dry environment, horizontally homogeneous, with no subsidence. The additional governing prognostic equations are (4.4.1b) for $\overline{u_i'u_j'}$, and (4.4.3c) for $\overline{w'\theta'}$. The resulting set of coupled equations is:

$$\frac{\partial \overline{U}_i}{\partial t} = -f_c \varepsilon_{ij3} (\overline{U}_{g_j} - \overline{U}_j) - \frac{\partial (\overline{u_i'w'})}{\partial z} \qquad (\text{for } i \neq 3) \qquad (6.6a)$$

$$\frac{\partial \overline{\theta}}{\partial t} = -\frac{\partial (\overline{w'\theta'})}{\partial z}$$

$$\frac{\partial \overline{e}}{\partial t} = -\overline{u'w'}\frac{\partial \overline{U}}{\partial z} - \overline{v'w'}\frac{\partial \overline{V}}{\partial z} + \left(\frac{g}{\overline{\theta}}\right)\overline{w'\theta'} - \frac{\partial \left[\overline{w'((p'/\overline{\rho}) + e)}\right]}{\partial z} - \varepsilon$$

$$\frac{\partial \left(\overline{\theta'^2}\right)}{\partial t} = -2\,\overline{w'\theta'}\frac{\partial \overline{\theta}}{\partial z} - \frac{\partial (\overline{w'\theta'^2})}{\partial z} - 2\varepsilon_\theta - \varepsilon_R$$

$$\frac{\partial (\overline{u_i'u_j'})}{\partial t} = -\overline{u_i'w'}\frac{\partial \overline{U}_i}{\partial z} - \overline{u_j'w'}\frac{\partial \overline{U}_i}{\partial z} - \frac{\partial (\overline{u_i'u_j'w'})}{\partial z} + \left(\frac{g}{\overline{\theta}}\right)\left[\delta_{i3}\overline{u_j'\theta'} + \delta_{j3}\overline{u_i'\theta'}\right]$$

$$+ \overline{\left(\frac{p'}{\rho}\right)\left[\frac{\partial u_i'}{\partial x_j} + \frac{\partial u_j'}{\partial x_i}\right]} - 2\varepsilon_{u_iu_j}$$

$$\frac{\partial (\overline{u_i'\theta'})}{\partial t} = -\overline{w'\theta'}\frac{\partial \overline{U_i}}{\partial z} - \overline{u_i'w'}\frac{\partial \overline{\theta}}{\partial z} - \frac{\partial (\overline{u_i'w'\theta'})}{\partial z} + \delta_{i3} g \frac{\overline{\theta'^2}}{\overline{\theta}} + \left(\frac{1}{\overline{\rho}}\right)\left[\overline{p'\frac{\partial \theta'}{\partial x_i}}\right] - \varepsilon_{u\theta}$$

The unknowns in this set of equations include pressure-correlation terms: $(1/\overline{\rho})[\overline{p'\,\partial\theta'/\partial x_i}]$, $\overline{(p'/\overline{\rho})\,[\partial u_i'/\partial x_j + \partial u_j'/\partial x_i]}$ and $\overline{w'p'}/\overline{\rho}$; third moments: $\overline{w'e}$, $\overline{w'\theta'^2}$, $\overline{u_i'w'\theta'}$, and $\overline{u_i'u_j'w'}$; and dissipation terms: ε, ε_R, ε_θ, $\varepsilon_{u\theta}$, $\varepsilon_{u_iu_j}$. Table 6-5 lists two different parameterizations (Deardorff, 1973; Donaldson, 1973) for some of these terms. Many other para-meterizations have appeared in the literature (Launder, et al., 1975; Lumley and Khajeh-Nouri, 1974; Mellor and Yamada, 1974; Wyngaard, et al., 1974; Mellor and Herring, 1973; Hanjalic and Launder, 1972; Lumley and Mansfield, 1984; Rotta, 1951; Schumann, 1977; Wyngaard, 1982; Zeman, 1981; Wichmann and Schaller, 1986; Wai, 1987).

Table 6-5. Sample second-order closure parameterizations suggested by (A) Donaldson, and (B) Deardorff. (Reference: Workshop on Micrometeorology, 1973). The Λ_i are length scales, which are either held constant or based on mixing-length arguments.

1

$$\overline{u_i'u_j'u_k'} = -\Lambda_2 e^{1/2}\left[\frac{\partial \overline{u_i'u_j'}}{\partial x_k} + \frac{\partial \overline{u_i'u_k'}}{\partial x_j} + \frac{\partial \overline{u_k'u_j'}}{\partial x_i}\right] \quad \text{(A)}$$

$$= -\frac{3}{2}\left(\frac{\Lambda_2}{e^{1/2}}\right)\left[\overline{u_k'u_m'}\frac{\partial \overline{u_i'u_j'}}{\partial x_m} + \overline{u_j'u_m'}\frac{\partial \overline{u_i'u_k'}}{\partial x_m} + \overline{u_i'u_m'}\frac{\partial \overline{u_k'u_j'}}{\partial x_m}\right] \quad \text{(B)}$$

2

$$\overline{u_i'u_j'\theta'} = -\Lambda_2 e^{1/2}\left[\frac{\partial \overline{u_i'\theta'}}{\partial x_j} + \frac{\partial \overline{u_j'\theta'}}{\partial x_i}\right] \quad \text{(A)}$$

$$= -\frac{3}{2}\left(\frac{\Lambda_2}{e^{1/2}}\right)\left[\overline{\theta'u_m'}\frac{\partial \overline{u_i'u_j'}}{\partial x_m} + \overline{u_j'u_m'}\frac{\partial \overline{u_i'\theta'}}{\partial x_m} + \overline{u_i'u_m'}\frac{\partial \overline{\theta'u_j'}}{\partial x_m}\right] \quad \text{(B)}$$

3

$$\overline{u_i'\theta'^2} = -\Lambda_2 e^{1/2}\left[\frac{\partial \overline{\theta'^2}}{\partial x_i}\right] \quad \text{(A)}$$

$$= -\frac{3}{2}\left(\frac{\Lambda_2}{\bar{e}^{1/2}}\right)\left[2\,\overline{\theta' u_m'}\,\frac{\partial \bar{u}_i}{\partial x_m} + \overline{u_i' u_m'}\,\frac{\partial \bar{\theta}^2}{\partial x_m}\right] \qquad \text{(B)}$$

4

$$\overline{\left(\frac{p'}{\bar{\rho}}\right)\left[\frac{\partial u_i'}{\partial x_j} + \frac{\partial u_j'}{\partial x_i}\right]} = -\left(\frac{\bar{e}^{1/2}}{\Lambda_1}\right)\left[\overline{u_i' u_j'} - \frac{2}{3}\delta_{ij}\bar{e}\right] \qquad \text{(Rotta, 1951) (A)}$$

$$= -\left(\frac{\bar{e}^{1/2}}{\Lambda_1}\right)\left[\overline{u_i' u_j'} - \frac{2}{3}\delta_{ij}\bar{e}\right] + \frac{2}{5}\bar{e}\left[\frac{\partial \bar{U}_i}{\partial x_j} + \frac{\partial \bar{U}_j}{\partial x_i}\right] \qquad \text{(B)}$$

5

$$\left(\frac{1}{\bar{\rho}}\right)\left[\overline{p'\frac{\partial \theta'}{\partial x_i}}\right] = -\left(\frac{\bar{e}^{1/2}}{\Lambda_1}\right)\overline{u_i'\theta'} \qquad \text{(A)}$$

$$= -\left(\frac{\bar{e}^{1/2}}{\Lambda_1}\right)\overline{u_i'\theta'} - \frac{1}{3}\delta_{13}\frac{g}{\bar{\theta}}\overline{\theta'^2} \qquad \text{(B)}$$

6

$$\frac{1}{\bar{\rho}}\left(\overline{p' u_i'}\right) = -\left(\frac{\bar{e}^{1/2}}{\Lambda_3}\right)\frac{\partial \overline{u_i' u_j'}}{\partial x_j} \qquad \text{(A,B)}$$

7

$$\varepsilon = \frac{\bar{e}^{3/2}}{\Lambda_4} \qquad \text{(A,B)}$$

8

$$\varepsilon_\theta = \frac{\bar{e}^{-1/2}\,\overline{\theta'^2}}{\Lambda_4} \qquad \text{(A,B)}$$

Note: the $\overline{w'e}$ parameterization is the same as that for $\overline{u_i' u_j' u_k'}$.

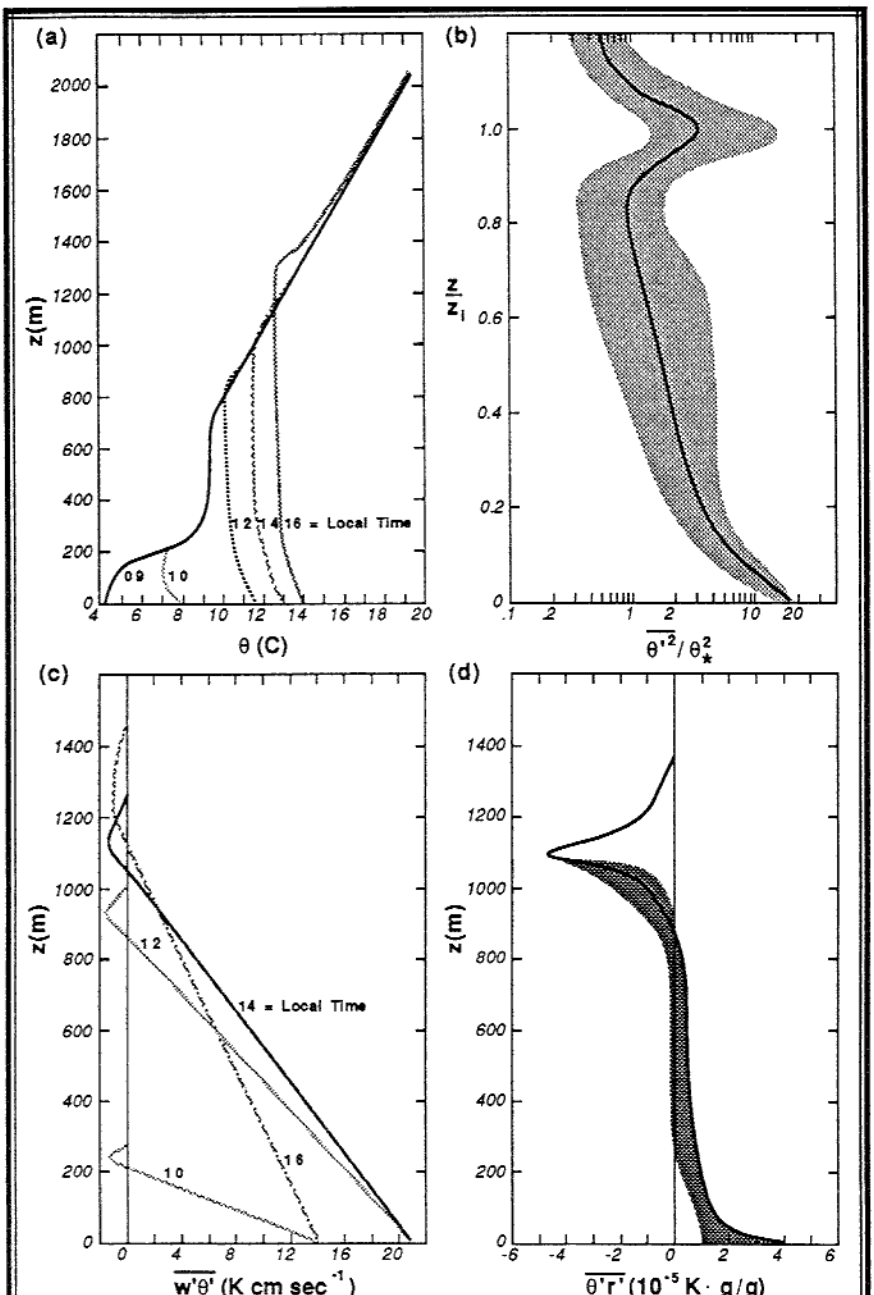

Fig. 6.7 Sample forecasts using second-order closure (from Sun and Ogura, 1980). Solid lines in (b) and (d) indicate model forecast; shaded areas show range of observed values.

There are three basic closure ideas contained in Table 6-5:

- ***Down-gradient diffusion*** (items 1-3 and 6 in the table), diffusion of the third-order statistics down the gradient of the second-order statistics;
- ***Return to isotropy*** (items 4 and 5), proportional to the amount of anisotropy;
- ***Decay*** (items 7 and 8), proportional to the magnitude of the turbulence.

A sample second-order closure model forecast is given in Fig 6.7, based on the moist convective boundary layer simulations of Sun and Ogura (1980). In addition to the equations listed above, they included prognostic equations for mixing ratio, $\bar{r}$, moisture variance $\overline{r'^2}$, moisture flux $\overline{w'r'}$, and temperature-moisture covariance, $\overline{r'\theta'}$. Using the full second-order set of equations, they could produce forecasts of mean variables (Fig 6.7a), as can be produced (with poorer accuracy) by first-order closure. They could forecast variances (Fig 6.7b), as can be produced (with poorer accuracy) by one-and-a-half-order closure. Most importantly, they can also produce forecasts of fluxes (Fig 6.7c) and other covariances (Fig 6.7d) that the lower-order schemes can not forecast.

6.7 Local Closure — Third Order

It is beyond the scope of this book to go into the details of third-order closure. In general, the prognostic equations for the triple-correlation terms are retained, while parameterizations are devised for the fourth-order correlations, for the pressure correlations, and for viscous dissipation. Some of the parameterizations presented in the literature (André, et al, 1978; Wyngaard, 1982; Moeng and Randall, 1984; Bougeault, 1981a, 1981b, 1985; Wichmann and Schaller, 1985; André and Lacarrere, 1985; Briere, 1987) assume that the fourth-order moments have a quasi-Gaussian probability distribution, and can be approximated as a function of second-moment terms. Any unrealistic values for some of the third moments are truncated or ***clipped*** to remain within physically realistic ranges, and various eddy damping schemes are used to prevent negative variances.

It is generally assumed that equations for lower-order variables (such as mean wind or fluxes) become more accurate as the closure approximations are pushed to higher orders. In other words, parameterizations for the fourth-order terms might be very crude, but there are enough remaining physics (unparameterized terms) in the equations for the third moments that these third moments are less crude. The second moment equations bring in more physics, making them even more precise — and so on down to the equations for the mean wind and temperature, etc. Based on the successful simulations published in the literature, this philosophy indeed seems to work.

Higher-order moments are extremely difficult to measure in the real atmosphere. Measurements of fluxes (second moments) typically have a large amount of scatter. Eddy correlation estimates of third moments are even worse, with noise or error levels larger than the signal level. Accurate fourth-order moment measurements are virtually nonexistent. This means that we have very little knowledge of how these third and fourth

moments behave; therefore, we have little guidance for suggesting good parameterizations for these moments. Now we see why such crude approximations are made in third-order closure models.

Higher-order closure models have many parameters that can be adjusted advantageously to yield good forecasts. These parameters are fine-tuned using special limiting case studies and laboratory flows where simplifications cause some of the terms to disappear, allowing better determination of the few remaining terms.

6.8 Nonlocal Closure — Transilient Turbulence Theory

Nonlocal closure recognizes that larger-size eddies can transport fluid across finite distances before the smaller eddies have a chance to cause mixing. This advective-like concept is supported by observations of thermals rising with undiluted cores, finite size swirls of leaves or snow, and the organized circulation patterns sometimes visible from cloud photographs.

Two first-order nonlocal closure models will be presented here. One, called ***transilient turbulence theory***, approaches the subject from a physical space perspective. The other, called ***spectral diffusivity theory***, utilizes a spectral or phase-space approach. Both allow a range of eddy sizes to contribute to the turbulent mixing process.

Two separate forms of transilient turbulence theory have evolved (Stull, 1984): one in discrete form for numerical modeling, and the other in analytical integral form for theoretical work. We will start with the discrete form because it is easier to picture physically.

6.8.1 Discrete Form — Definition of Framework

Imagine a one-dimensional column of air that is split into separate equal-size grid boxes, as sketched in Fig 6.8a. In a numerical model, grid point locations in the center of each box represent the average conditions within those boxes. If we focus on just one particular (reference) grid box, we can identify those eddies that mix air into our reference box from other boxes above and below, and we can locate the destination boxes for air that leaves the reference box. This same procedure can be used to investigate mixing between all boxes in the column, as shown by the superposition of eddies in Fig 6.8b.

Turbulent mixing of fluid into our reference box (the box with index i) from the other boxes can change the state (temperature, humidity, tracer concentration, etc.) of that box.

For example, let $\overline{\xi}_i$ represent the average concentration of passive tracer in our reference box, i. If c_{ij} represents the fraction of air in box i that came from box j during a time interval Δt, then we need only sum the mixing from over all N grid boxes in the column to find the new concentration at box i:

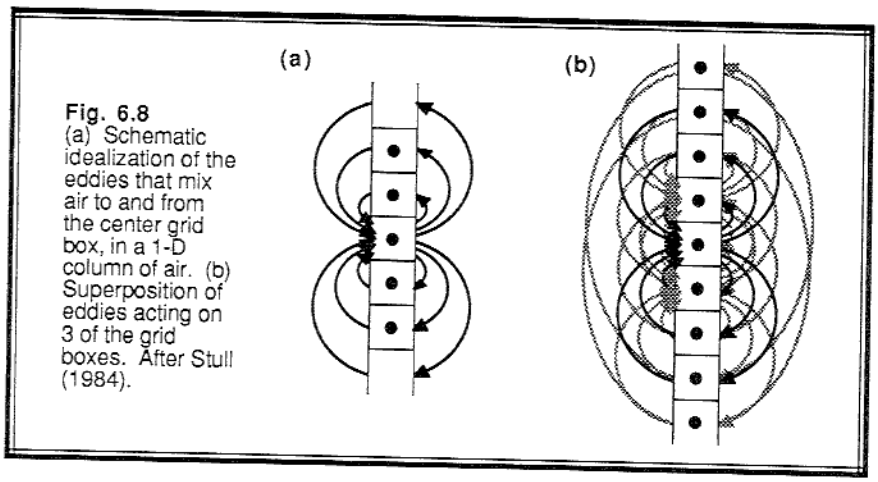

Fig. 6.8
(a) Schematic idealization of the eddies that mix air to and from the center grid box, in a 1-D column of air. (b) Superposition of eddies acting on 3 of the grid boxes. After Stull (1984).

$$\bar{\xi}_i(t + \Delta t) = \sum_{j=1}^{N} c_{ij}(t, \Delta t)\, \bar{\xi}_j(t) \qquad (6.8.1)$$

This equation says that when air is mixed into box i from box j, the air carries with it an amount c_{ij} of the tracer with concentration $\bar{\xi}_j$. The coefficient c_{ii} represents the fraction of air in box i that remains within box i.

Although (6.8.1) was developed for just one reference box, it is general enough to work for any and all equal-size boxes. If we recognize that c_{ij} is an NxN matrix of mixing coefficients (called a ***transilient matrix***), and $\bar{\xi}_j$ is a Nx1 matrix (i.e., a vector) of concentrations, then it is obvious that (6.8.1) describes simple matrix multiplication.

When eddies move parcels of air from one grid box to another, the air will carry with it not only the tracer concentration, but the heat, moisture, momentum and other measures of the state of the fluid. Hence, (6.8.1) can be used for any of these variables, where the transilient matrix is the same for each variable (i.e., it changes only with time and timestep). Of course, the $\bar{\xi}_j$ vector is different for each variable.

A variety of physical processes can be modeled with the transilient scheme depending on the form of the transilient matrix. Idealized examples of complete mixing, small-eddy mixing (like K-theory), a detraining updraft core, patchy turbulence, no turbulence, and eddies triggered by the surface layer are illustrated in Fig 6.9a.

Fig 6.9b shows measurements (Ebert et al., 1989) of the transilient matrix for a convective ML, with a less-turbulent FA above it. Contoured values of the matrix are presented rather than the raw numbers, and the matrix is flipped upside-down so that the vertical coordinate corresponds to height increasing upward in the atmosphere. Not only is the mixing very nonlocal, but the matrix is asymmetric. Also in this figure is a diagram indicating the interpretation of such transilient matrices.

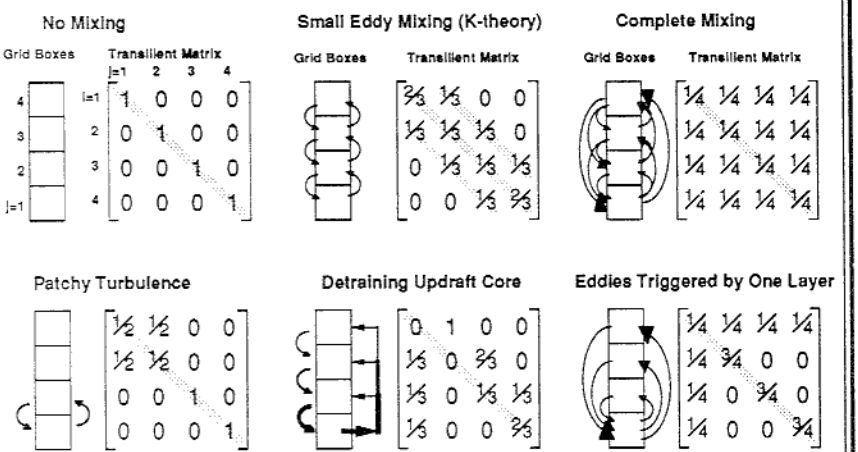

Fig. 6.9 a Examples of idealized transilient matrices showing nonlocal mixing possibilities. The arrows are not physical eddies, but they represent the net mixing effect of many real eddies acting in 3-D space. Grid index conventions are indicated in the top left drawing.

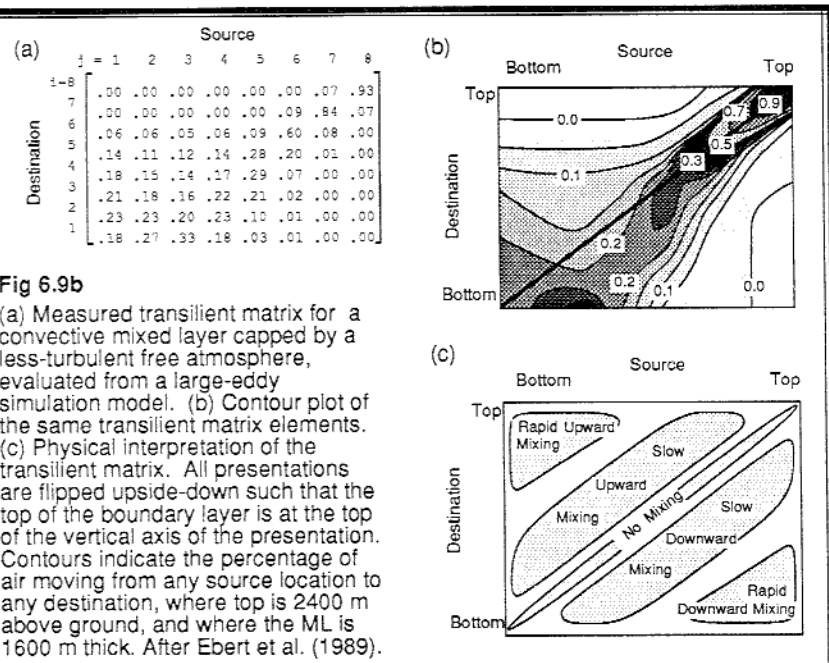

Fig 6.9b
(a) Measured transilient matrix for a convective mixed layer capped by a less-turbulent free atmosphere, evaluated from a large-eddy simulation model. (b) Contour plot of the same transilient matrix elements. (c) Physical interpretation of the transilient matrix. All presentations are flipped upside-down such that the top of the boundary layer is at the top of the vertical axis of the presentation. Contours indicate the percentage of air moving from any source location to any destination, where top is 2400 m above ground, and where the ML is 1600 m thick. After Ebert et al. (1989).

6.8.2 Physical Constraints

If the total amount of air within the reference box does not change with time, then just as much air must leave the box during Δt as enters. Expressed in another way, if c_{ij} is the fraction of air entering box i from box j, then by definition the ***conservation of air mass*** requires that the sum over j of all mixing fractions be unity:

$$1 = \sum_{j=1}^{N} c_{ij} \tag{6.8.2a}$$

One way to visualize this is to picture a column of air with initially the same tracer concentration in each box. We known that after any amount of mixing, the final concentration in any of the boxes must equal the initial concentration: $\bar{\xi}_j = \bar{\xi}_i = \sum_{j=1}^{N} c_{ij} \bar{\xi}_j$. This is satisfied by (6.8.2a).

Also, if the amount of tracer initially in box j is conserved as it mixes out of j and into the other boxes, i, then ***conservation of tracer amount*** requires that:

$$1 = \sum_{i=1}^{N} c_{ij} \tag{6.8.2b}$$

One way to appreciate this constraint is to picture a column of air with no tracers in any box, except for a unit amount of tracer in one box ($\bar{\xi}_j = 1$). If all of the tracer is initially in box j, then after the mixing associated with one timestep, some of this tracer could be mixed into any or all of the other boxes. Nevertheless, the total amount of tracer in all boxes must still sum to unity ($\sum_{i=1}^{N} \bar{\xi}_i = 1$). The only way that this is possible given mixing defined by (6.8.1) is if (6.8.2b) is true.

We see that (6.8.2a & b) are conservation constraints for air mass and tracer mass. In addition, none of the individual elements c_{ij} should be allowed to be negative, otherwise turbulence would cause "unmixing" and would decrease randomness or entropy. Thus, each element of the matrix must be $0 \le c_{ij} \le 1$, and each row and each column must sum to one. Such a matrix is sometimes called a ***doubly stochastic matrix***.

6.8.3 Numerical Constraints.

One ancillary feature of the physical constraints is that a numerical forecast based on transilient turbulence theory is ***absolutely numerically stable*** for any size timestep

and any size grid spacing (Stull, 1986). No additional numerical constraints are required to achieve this characteristic.

To show this, we can employ Gershgorin's theorem of linear algebra (Pearson, 1974) that states that the largest modulus (magnitude) of any of the eigenvalues of the transilient matrix is no greater than the largest sum of any row or column of our non-negative matrix. Because each of our rows and columns sum to one, we know that the largest eigenvalue modulus is no greater than one. This latter condition means that numerical stability is insured. See Haltiner and Williams (1980) for details of this last statement.

There is one numerical constraint that is recommended: that no eigenvalue of the transilient matrix be negative. It can be shown that a transilient matrix with a negative eigenvalue causes the tracer concentration to oscillate from timestep to timestep. This characteristic is undesirable because the solution depends on the timestep rather than the physics. As a general guideline, transilient matrices with large elements clustered around the cross-diagonal of the matrix rather than around the main diagonal are matrices likely to be timestep dependent.

6.8.4 Flux Determination

Turbulent kinematic fluxes are also easy to determine, because the transilient matrix tells us directly about the transport between grid boxes. The kinematic flux $\overline{w'\xi'}(k)$ across level k is given by:

$$\overline{w'\xi'}(k) = \left(\frac{\Delta z}{\Delta t}\right) \sum_{i=1}^{k} \sum_{j=1}^{N} c_{ij} \left(\bar{\xi}_i - \bar{\xi}_j\right) \qquad (6.8.4a)$$

where Δz is the grid point spacing, and Δt is the timestep interval for the $c_{ij}(t,\Delta t)$ matrix. The level k is defined as the border between grid boxes k and k+1. Thus, although $\bar{\xi}_i$ is known at the center of a grid box, $\overline{w'\xi'}(k)$ is known at the edge of the grid box. This makes physical sense, because the flux represents the transport between grid boxes.

We expect that the flux across any level k should depend on only those eddies that cross that level (Ebert et al, 1989). When (6.8.4a) is rewritten as (6.8.4b), we see that one of the sums is from 1 to k, while the other is from k+1 to N. This implies that the source and destination grid boxes of those eddies that contribute to the flux are below and above k, respectively.

$$\overline{w'\xi'}(k) = \frac{\Delta z}{\Delta t} \sum_{i=1}^{k} \sum_{j=k+1}^{N} \left[c_{ji} \bar{\xi}_i - c_{ij} \bar{\xi}_j \right] \qquad (6.8.4b)$$

An outline is given here for the derivation of (6.8.4a). First, start with a simple conservation equation where the only forcing is vertical flux divergence: $\partial\bar{\xi}/\partial t = -\partial\overline{w'\xi'}/\partial z$. Integrate this over one timestep, from t to t+Δt, and rewrite the result as $\partial\overline{w'\xi'}^{\Delta t}/\partial z = [\,\bar{\xi}(t) - \bar{\xi}(t+\Delta t)]\,/\,\Delta t$. Next, integrate this from the surface (z=0) to the height of interest where the flux is desired (z=Z), where $Z = k\,\Delta z$. By splitting the integral of the right side of the equation into the sum of smaller integrals, where each small integral is over one grid box of depth Δz, our equation now becomes $\overline{w'\xi'}^{\Delta t}(Z) - \overline{w'\xi'}^{\Delta t}(0) = (\Delta z/\Delta t)\sum_{i=1}^{k}[\,\bar{\xi}_i(t) - \bar{\xi}_i(t+\Delta t)\,]$. But the turbulent flux across a solid boundary, or into any nonturbulent part of the atmosphere, is zero by definition, making the second term on the left become zero. Also, the term in square brackets can be written using (6.8.1) and (6.8.2a) as $[\sum_{j=1}^{N} c_{ij}\bar{\xi}_i - \sum_{j=1}^{N} c_{ij}\bar{\xi}_j]$. A bit of algebraic manipulation puts the final result into the form of (6.8.4a).

As just stated, the turbulent flux across a solid boundary is zero by definition, even though the nonturbulent fluxes might not be zero (see Section 7.1 for a discussion of effective fluxes). Thus, $\overline{w'\xi'}(k=0) \equiv 0$. With this boundary condition, (6.8.4a) can be rewritten as a recursion relationship:

$$\overline{w'\xi'}(k) = \overline{w'\xi'}(k-1) + \left(\frac{\Delta z}{\Delta t}\right)\sum_{j=1}^{N} c_{kj}\left(\bar{\xi}_k - \bar{\xi}_j\right) \qquad (6.8.4c)$$

6.8.5 Example of Transilient Framework

Problem: Suppose that we start with a shallow mixed layer of depth 300 m within a 500 m column of air, with initial profiles of potential temperatures and winds as indicated below. Assume the column is divided into five equal-thickness (100 m) grid boxes.

Profile A:

Given:							
Grid index	=	1	2	3	4	5	
z (m)	=	50	150	250	350	450	(At the box centers)
$\bar{\theta}$ (°C)	=	15	15	15	16	18	
$\bar{U}$ (m/s)	=	5	5	5	7	6	

Next, assume that there are molecular (nonturbulent) fluxes of heat, $Q_H = 0.2$ K m/s, and momentum, $F = -0.15$ m^{2}s^{-2}, across the land surface into the air. During a 10 min timestep, we can assume that there is a surface molecular flux into the bottom of the bottom layer, but no molecular flux out of the top of the bottom layer, giving $\Delta\theta_1/\Delta t = Q_H/\Delta z$ and $\Delta U_1/\Delta t = F/\Delta z$. Neglecting other forcings such as radiation and Coriolis force leaves only the bottom layer altered:

Profile B:

Given:	Grid index =	1	2	3	4	5
	z (m) =	50	150	250	350	450
	$\overline{\theta}$ (°C) =	16.2	15	15	16	18
	$\overline{U}$ (m/s) =	4.1	5	5	7	6

Notice that only the bottom one grid box has changed so far, because we have not yet applied the transilient turbulence to mix these heat and momentum changes higher in the mixed layer.

Next, assume that there is turbulent mixing during the 10 min period as specified by the transilient matrix below:

$$\mathbf{c}\ (t, \Delta t = 10\ \text{min}) = \begin{array}{c} (j= \quad 1 \quad\ 2 \quad\ 3 \quad\ 4 \quad\ 5\ ) \\ \left[\begin{array}{ccccc} 0.590 & 0.236 & 0.118 & 0.056 & 0.000 \\ 0.236 & 0.590 & 0.118 & 0.056 & 0.000 \\ 0.118 & 0.118 & 0.708 & 0.056 & 0.000 \\ 0.056 & 0.056 & 0.056 & 0.832 & 0.000 \\ 0.000 & 0.000 & 0.000 & 0.000 & 1.000 \end{array}\right] \end{array} \begin{array}{l} (i=1) \\ (2) \\ (3) \\ (4) \\ (5) \end{array}$$

Starting with Profile B, (a) determine and plot the final profile (let's call it Profile C) after turbulent mixing; and (b) determine and plot the fluxes of heat and momentum.

Solution to part (a): First, it is easy to verify that the transilient matrix is a valid one, with each row and column summing to one, and no negative elements. Next, to illustrate the solution, look at the second row of the transilient matrix. The second row tells us about fluid that is mixing ***into*** the second grid box. For our case, it says that 23.6% comes ***from*** box 1, 59% stays in box 2, 11.8% comes from box 3, and so forth. Thus, the new state of box two after mixing is:

$$\overline{\theta}_2 = 0.236\cdot(16.2) + 0.590\cdot(15) + 0.118\cdot(15) + 0.056\cdot(16) + 0.000\cdot(18) = 15.34\ (°C)$$

and

$$\overline{U}_2 = 0.236\cdot(4.1) + 0.590\cdot(5) + 0.118\cdot(5) + 0.056\cdot(7) + 0.000\cdot(6) = 4.90\ (\text{m/s})$$

In general we can set up the problem as a matrix multiplication, with the answer indicated below for potential temperature. The same procedure can be used for winds.

$$\begin{bmatrix} 15.76 \\ 15.34 \\ 15.20 \\ 15.90 \\ 18.00 \end{bmatrix} = \begin{bmatrix} 0.590 & 0.236 & 0.118 & 0.056 & 0.000 \\ 0.236 & 0.590 & 0.118 & 0.056 & 0.000 \\ 0.118 & 0.118 & 0.708 & 0.056 & 0.000 \\ 0.056 & 0.056 & 0.056 & 0.832 & 0.000 \\ 0.000 & 0.000 & 0.000 & 0.000 & 1.000 \end{bmatrix} \begin{bmatrix} 16.2 \\ 15.0 \\ 15.0 \\ 16.0 \\ 18.0 \end{bmatrix}$$

Profile C: The state of the air after 10 minutes.

Given:	Grid index =	1	2	3	4	5	
	z (m) =	50	150	250	350	450	(At the box centers)
	$\overline{\theta}$ (°C) =	15.76	15.34	15.20	15.90	18.00	
	$\overline{U}$ (m/s) =	4.58	4.90	5.01	6.61	6.00	

Discussion of part (a): The new temperature in grid box 5 has not changed, because the fifth element along the main diagonal of the transilient matrix equalled one. Thus, 100% of the air in box 5 stayed in box 5, and no air was mixed in from other boxes. The initial and final potential temperature and wind profiles are plotted in Figs 6.10 a & b.

Some of the warm air from the surface has been mixed up into the mixed layer, resulting in warming of the mixed layer and a reduction of the static instability between the bottom two grid points. Also, there appears to be some entrainment into the top of the mixed layer, resulting in an increase in mixed layer depth.

Solution to part (b): For example, the flux at z=100 m (i.e., at k=1, between grid points 1 and 2) can be found using recursive relationship (6.8.4b):

$$\overline{w'\theta'}(1) = \overline{w'\theta'}(0) + \frac{\Delta z}{\Delta t} \sum_{j=1}^{N} c_{1j} \left(\overline{\theta}_1 - \overline{\theta}_j \right)$$

$$\overline{w'\theta'}(1) = 0 + (100 \text{ m} / 600 \text{ s}) \cdot [0.590 \cdot (16.2-16.2) + 0.236 \cdot (16.2-15.0) + 0.118 \cdot (16.2-15.0) + 0.056 \cdot (16.2-16.0) + 0.000 \cdot (16.2-18.0)]$$

$$= 0.0726 \text{ (K·m·s}^{-1}\text{)}$$

and for momentum

$$\overline{u'w'}(1) = 0 + (100 \text{ m} / 600 \text{ s}) \cdot [0.590 \cdot (4.1-4.1) + 0.236 \cdot (4.1-5.0) + 0.118 \cdot (4.1-5.0) + 0.056 \cdot (4.1-7.0) + 0.000 \cdot (4.1-6.0)]$$

$$= -0.080 \text{ (m}^2\text{s}^{-2}\text{)}$$

Similarly, the turbulent fluxes between the other grid points can be found:

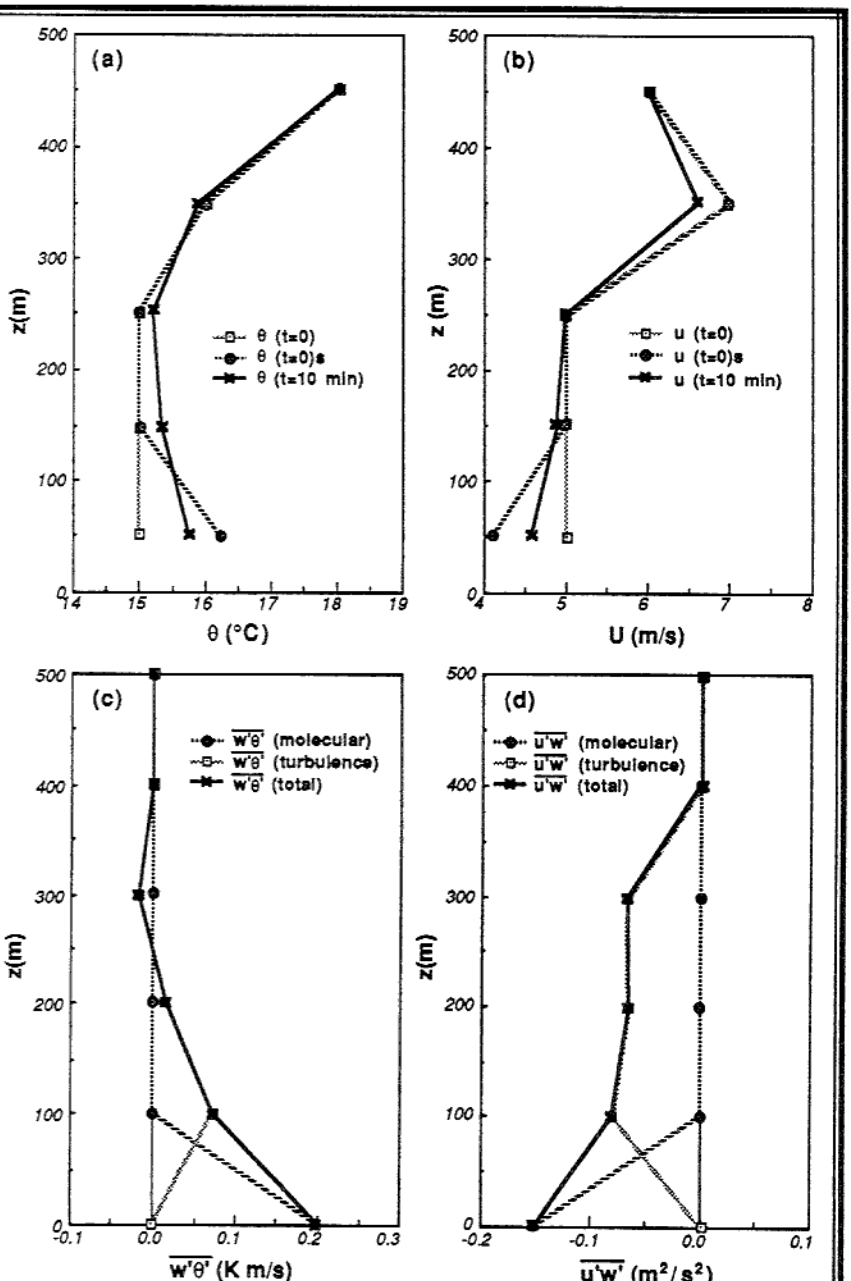

Fig. 6.10 Examples of: (a) potential temperature evolution (b) mean wind evolution, (c) heat flux, (d) and momentum flux soundings using transilient turbulence (Stull, 1987a).

Grid index =	0	1	2	3	4	5
z (m) =	0	100	200	300	400	500
$\overline{w'\theta'}$(K m/s) =	0	0.0726	0.0160	-0.0169	0.0	0.0
$\overline{u'w'}$(m^2s^{-2}) =	0	-0.0802	-0.0634	-0.0644	0.0	0.0

Discussion of part (b): These flux profiles are plotted in Figs 6.10 c & d. In addition to the turbulent fluxes in these figures, the molecular surface fluxes are also plotted. The total flux at any height is the sum of the turbulent and molecular fluxes, as indicated by the solid lines. It is this total flux that is usually plotted as the effective flux in the meteorological literature (see Chapter 7).

The heat flux profile shows the expected decrease of flux with height characteristic of convective mixed layers, with a negative value in the entrainment zone. The momentum flux profile is negative at all heights, implying a loss of momentum down to the ground.

6.8.6 Closure Parameterization

Like other turbulence closure schemes, a parameterization must be devised for the unknowns: the c_{ij} coefficients. Two closure methods have been used in the literature: an ***a-priori*** method that utilizes knowledge or assumptions about the turbulence spectrum or about the frequency distribution of turbulent velocities; and a ***responsive*** approach that allows the transilient coefficients to change in response to changes in the mean flow. The a-priori method is used with the spectral diffusivity nonlocal closure described at the end of this Chapter. The responsive approach will be described here.

The underlying concept behind the responsive closure is that if the fluid is made statically or dynamically unstable, then turbulence will form to partially undo the instability by mixing. This is analogous to LeChatelier's Principle of chemistry.

This principle is carried into the numerical implementation of transilient turbulence theory, as sketched in the time line of Fig 6.11. Each timestep is split into two parts, one part that includes all the nonturbulent dynamics, thermodynamics, boundary conditions, and internal (body) forcings. The second part is where the transilient turbulence closure algorithm responds to the instabilities in the mean flow field by causing mixing, where the amount of mixing is given by transilient coefficients that are parameterized to (partially) undo the mean flow instabilities. This two step process was illustrated in the previous example, where the surface fluxes were first applied to destabilize the flow, and then the transilient mixing was applied.

The following responsive parameterization (Stull and Driedonks, 1987) for c_{ij} is based on a dimensionless ***mixing potential*** between grid points i and j, Y_{ij}:

$$c_{ij} = \frac{Y_{ij}}{\| Y \|} \qquad \text{for } i \neq j \qquad (6.8.6a)$$

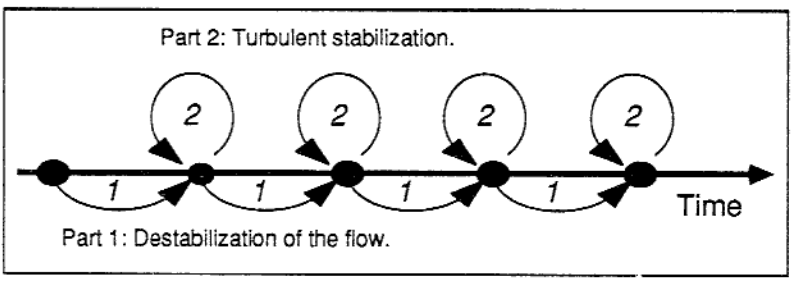

Fig. 6.11 Timeline showing the two parts of the responsive parameterization. Part 1 consists of the dynamics, thermodynamics, body forcing and boundary conditions. Part 2 consists of the transilient mixing to reduce any flow instabilities that might have developed during part 1. After Stull (1987).

where ||Y|| is a scalar norm of matrix Y, and:

$$c_{ii} = 1 - \sum_{\substack{j=1 \\ j \neq i}}^{N} c_{ij} \qquad (6.8.6b)$$

to satisfy the conservation constraint discussed earlier.

The potential for mixing depends on the instability of the flow, so a natural starting point for the parameterization of Y is the TKE equation. Start with (5.1b), neglect the turbulent transport and pressure correlation terms for now, allow for an arbitrary coordinate direction, integrate over time, and then normalize the resulting equation by dividing by the TKE. Next, and most importantly, we hypothesize that the result can be interpreted nonlocally, where gradients can be expressed as differences across finite distances. Let Δ_{ij} refer to a nonlocal difference between grid points i and j; for example, $\Delta_{ij}\overline{U} = \overline{U}_i - \overline{U}_j$. We can finally write the equation for potential for mixing between grid points i and j, for $i \neq j$:

$$Y_{ij} = \left[\frac{\Delta t\, T_o}{(\Delta_{ij} z)^2}\right]\left[(\Delta_{ij}\bar{U})^2 + (\Delta_{ij}\bar{V})^2 - g(\Delta_{ij}\bar{\theta}_v)\frac{(\Delta_{ij} z)}{(\theta_v R_c)}\right] - \frac{D_Y \Delta t}{T_o} \qquad (6.8.6c)$$

The first two terms on the right represent the mechanical production, the third term is the buoyant production/consumption, and the last term represents dissipation.

The Y_{ij} values found from (6.8.6c) are the preliminary off-diagonal elements of a **Y** matrix. We recommend that the mixing potential for eddies of any size be no less than the mixing potential for larger size eddies. In other words, if there is strong mixing between

100 m and 500 m, then there is at least as much mixing between 200 m and 300 m. It would be ridiculous to allow turbulence to mix fluid between two distant points across an interior region that was nonturbulent. Thus, we make the additional requirement that the elements of the **Y** matrix increase monotonically from the upper-right and lower-left corners toward the main diagonal. Any of the preliminary elements that do not satisfy this last requirement are increased to equal the largest elements further away from the diagonal. The elements along the main diagonal are set equal the the largest immediate element on the same row, plus a Y_{ref} value that represents the potential for subgrid scale mixing within one box.

If we assume that the mixing between i and j equals the mixing between j and i, then both the mixing potential matrix and the transilient matrix are symmetric. This reduces the degrees of freedom from $(N^2 - N)$ to $(N^2 - N)/2$. By using the mixing potential parameterization just described, we further reduce the degrees of freedom to just four, based on the four empirical parameters. Their values are recommended (based on atmospheric simulation tests) to be $T_o = 1000$ s, $D_Y = 1$ (dimensionless), the critical Richardson number is $R_c = 0.21$, and $Y_{ref} = 1000$ (dimensionless).

Finally, if each row of the final mixing potential matrix is summed, the scalar norm is set equal to the maximum sum. Namely,

$$\|Y\| = \max_i \left[\sum_{j=1}^{N} Y_{ij} \right] \qquad (6.8.6d)$$

Fig 6.12 shows an example of a boundary layer forecast made with the parameterization above. The growth of an entraining mixed layer is clearly evident, even though no explicit mixed layer or boundary layer specification was imposed other than the surface heating that acted on the bottom one grid point. The corresponding wind and flux forecasts for this case are shown by Stull and Driedonks (1987).

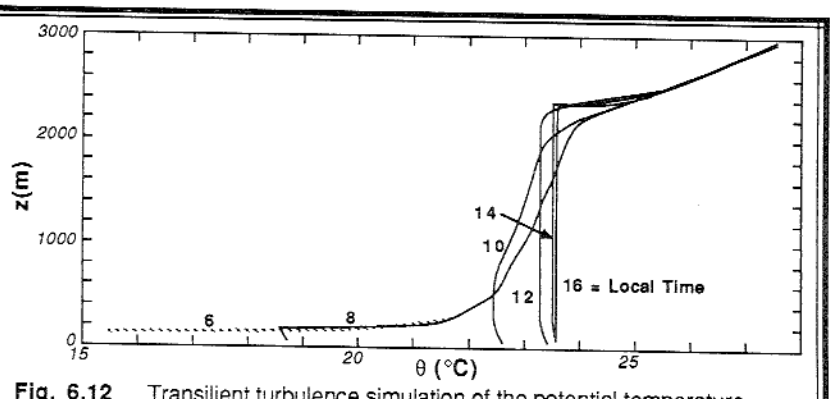

Fig. 6.12 Transilient turbulence simulation of the potential temperature profile evolution at Cabauw, Holland, for 30 May 1978. After Stull & Driedonks (1987).

6.8.7 Continuous Form

The analytical form of transilient turbulence theory can be written as

$$\frac{\partial \bar{\xi}(z,t)}{\partial t} = \text{TM} + \text{Prod.} - \text{Loss} \qquad (6.8.7a)$$

where Prod. and Loss are other production and loss terms, respectively, given by the conservation equations. The turbulent mixing (flux divergence) term, TM, is:

$$\text{TM}(z,t) = \int_{Z=z_b}^{z_t} \left[\bar{\xi}(Z,t) - \bar{\xi}(z,t) \right] \gamma_T(z,Z,t)\, dZ \qquad (6.8.7b)$$

where $\gamma_T(z,Z,t)$ is a transilient rate coefficient (units of $s^{-1}m^{-1}$) for mixing between level Z and level z. To help understand $\gamma_T(z,Z,t)$, we note that the kinematic mass flux of air moving from Z+Δz to z+Δz is $M = \iint \gamma(z,Z,t)dz\, dZ$. The top and bottom of the turbulent domain are at $z=z_b$ and z_t, respectively.

A typical shape for $\gamma_T(z,Z,t)$ is shown in Fig 6.13. This graph is similar to a graph of the magnitudes of the c_{ij} elements along any one row of the transilient matrix, where i=j (main diagonal) corresponds to z-Z=0.

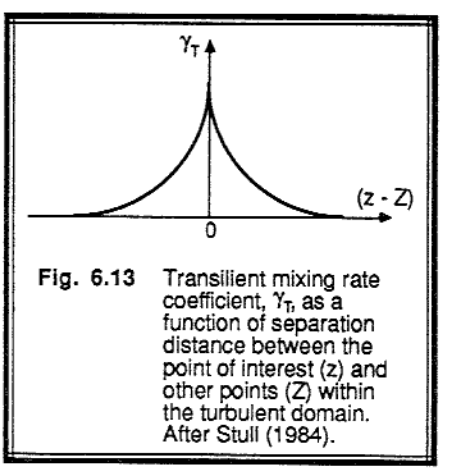

Fig. 6.13 Transilient mixing rate coefficient, γ_T, as a function of separation distance between the point of interest (z) and other points (Z) within the turbulent domain. After Stull (1984).

The turbulent kinematic flux, $\overline{w'\xi'} = F(z_1)$ at location z_1 is given by:

$$\overline{w'\xi'}(z_1,t) = \int_{z=z_b}^{z_1} \int_{Z=z_b}^{z_t} \left[\bar{\xi}(Z,t) - \bar{\xi}(z,t)\right] \gamma_T(z,Z,t)\, dZ\, dz \qquad (6.8.7c)$$

By definition, the turbulent flux at the top and bottom of the turbulent domain is zero.

6.8.8 Example of Continuous Form

Problem: Given the idealized transilient rate curve shown in Fig 6.14a, and the initial sounding of potential temperature shown in Fig 6.14b, calculate the initial tendency, $\partial\bar{\theta}/\partial t$ from (6.8.7a), neglecting other production and loss terms. The initial potential temperature sounding below the temperature jump (i.e., at $z<0$, assuming the origin is placed at the height of the jump) is constant and equal to $\bar{\theta}_o$, while above that height the temperature is $\bar{\theta}_o + \Delta\bar{\theta}$. The transilient rate curve is zero everywhere, except $\gamma_T = (A/L)(L - Z + z)$ for $0 < (Z-z) < L$, and $\gamma_T = (A/L)(L + Z - z)$ for $-L < (Z-z) < 0$.

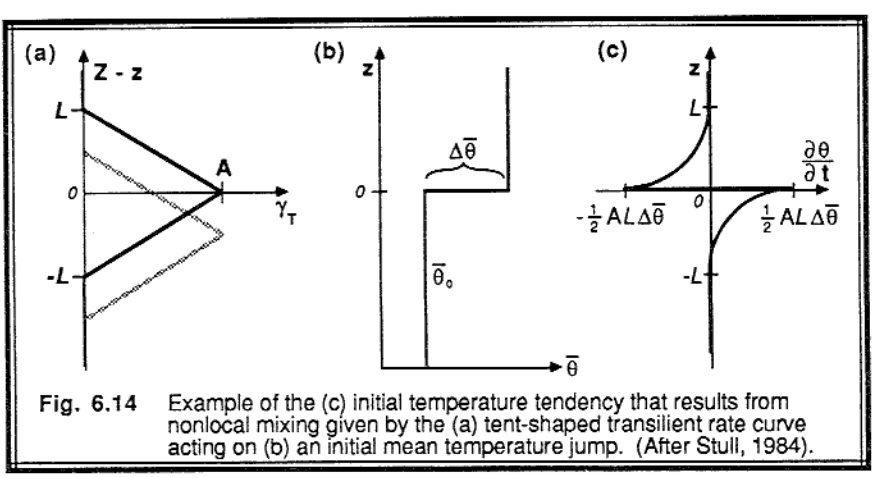

Fig. 6.14 Example of the (c) initial temperature tendency that results from nonlocal mixing given by the (a) tent-shaped transilient rate curve acting on (b) an initial mean temperature jump. (After Stull, 1984).

Solution: The transilient rate curve indicates that the largest eddies (i.e., large values of $|Z - z|$) present for this case are of size L. Thus, for $z < -L$ and $z > L$, mixing can not change the temperature because the smaller eddies (less than L) are mixing air of the same temperature. Air of different temperature from the other side of the temperature jump is out of reach of these small eddies. Thus, by inspection we can write the first part of our answer:

For $z < -L$ and $L < z$:

$$\frac{\partial \bar{\theta}}{\partial t} = 0 \qquad \text{for} \begin{cases} z > L \\ z < -L \end{cases}$$

For $-L < z < 0$:

We must integrate (6.8.7b), using the initial condition that $\bar{\theta}(Z) - \bar{\theta}(z)$ equals 0 for $Z < 0$, and equals $\Delta\bar{\theta}$ for $Z > 0$. Thus, the initial (t=0) tendency of potential temperature is:

$$\frac{\partial \bar{\theta}}{\partial t}(z) = TM = \int_{Z=z_b}^{z_T} \left[\bar{\theta}(Z) - \bar{\theta}(z) \right] \gamma_T(Z,z)\, dZ$$

$$= \frac{A}{L} \int_{Z=z_b}^{0} [0]\, \gamma_T dZ + \frac{A}{L} \int_{Z=0}^{z+L} [\Delta\bar{\theta}]\, (L - Z + z)\, dZ + \frac{A}{L} \int_{Z=z+L}^{z_T} [\Delta\bar{\theta}]\, (0)\, dZ$$

$$= \frac{A\ \Delta\bar{\theta}}{2\ L} (L+z)^2$$

For $0 < z < L$:
Integrating in a similar manner we find:

$$\frac{\partial \bar{\theta}}{\partial t}(z) = -\frac{A\ \Delta\bar{\theta}}{2\ L} (L-z)^2$$

Discussion: These initial tendencies are plotted in Fig 6.14c. Just above the temperature jump the tendency is negative, indicating cooling. Just below the jump, there is warming. The net result is that turbulence is tending to round the corners of the temperature sounding by mixing cooler air up and warmer air down. Also, these initial tendencies are nonzero a finite distance away from the jump, something that can not be modeled with a local closure theory such as K-theory.

6.8.9 Closure Parameterization of the Continuous Form

In order to close the continuous form of transilient turbulence theory, we need to find an analytical expression for γ_T as a function of z, Z, and t. One easy way to do this employs the a-priori method of closure: namely, assuming some turbulent state of the air

rather than letting it respond to changes in the mean flow. For example, given the spectrum of turbulence with an inertial subrange, it can be shown (Stull, 1984) that

$$\gamma_T(z,Z,t) \propto \varepsilon^{1/3} |Z-z|^{-5/3} \tag{6.8.9}$$

where ε is the TKE dissipation rate. Many other closure parameterizations can be formulated that lead to interesting theoretical results.

6.9 Nonlocal Closure — Spectral Diffusivity Theory

We saw in Section 6.4.1 that K-theory can be used to approximate a flux as $\overline{w'\xi'} = -K \partial\bar{\xi}/\partial z$. When this is put back into the conservation equation for a passive tracer, $\partial\bar{\xi}/\partial t = -\partial\overline{w'\xi'}/\partial z$, we arrive at the diffusion equation $\partial\bar{\xi}/\partial t = K\, \partial^2\bar{\xi}/\partial z^2$, where we have assumed that K is not a function of z for simplicity. Suppose that K varies with eddy size (Berkowicz and Prahm, 1979; Prahm et al., 1979; Berkowicz, 1984). If we let κ=wavenumber of the eddy, then we can spectrally decompose the diffusion equation to be

$$\frac{\partial\bar{\xi}(\kappa)}{\partial t} = K(\kappa)\frac{\partial^2\bar{\xi}(\kappa)}{\partial z^2} \tag{6.9a}$$

where $K(\kappa)$ is called the ***spectral turbulent diffusivity.***

By integrating this equation over all wavenumbers, we again arrive at the forecast equation for $\bar{\xi}$:

$$\frac{\partial\bar{\xi}(z,t)}{\partial t} = \text{TM} + \text{Prod.} - \text{Loss}$$

where the turbulent mixing term is now

$$\text{TM}(z,t) = \frac{\partial \int \left[\Xi(z,Z,t) \frac{\partial\bar{\xi}(Z)}{\partial Z} \right] dZ}{\partial z} \tag{6.9b}$$

and where the integration is over the domain of turbulence. The similarity of this to (6.8.7b) is striking. $\Xi(z,Z,t)$, which has units of m/s, is called the ***turbulent diffusivity transfer function***, and is defined by:

$$\Xi(z,Z,t) = \frac{1}{2\pi} \int K(\kappa,t) \exp\left[i\kappa(z - Z)\right] d\kappa \qquad (6.9c)$$

where i is the square root of -1 (see Chapter 8 for more details about Fourier analysis), and where the integration is over all wavenumbers, from $\kappa = -\infty$ to $+\infty$.

To use this nonlocal approach, we must parameterize either $K(\kappa)$ or Ξ. Berkowicz & Prahm suggested that larger eddies are more effective at causing diffusion (i.e., have larger K) than smaller eddies (see Fig 6.15). Based on this concept, they suggested that

$$K(\kappa) = \frac{K_o}{\left[1 + B_o \kappa^{4/3}\right]} \qquad (6.9d)$$

where the two parameters, K_o and B_o, are both assumed to be proportional to the 4/3 power of the wavelength at the peak in the TKE energy spectrum. In other words, this is an ***a-priori*** approach, where some knowledge of the spectrum of turbulence is assumed. K_o has units of $m^2\ s^{-1}$, while B_o has units of $m^{-4/3}$. This spectral dependence of K yields a plot of $\Xi(z,Z,t)$ vs. $(z-Z)$ that looks very similar to the plot of $\gamma(z,Z,t)$ in Fig 6.13, with a peak of Ξ at $z-Z = 0$ and tails that approach zero at both sides.

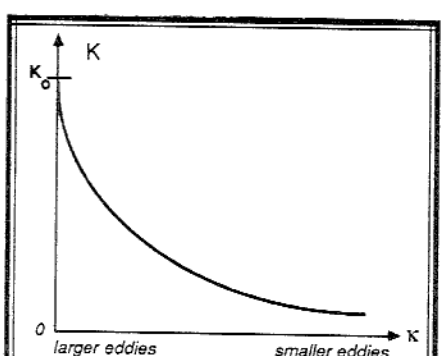

Fig. 6.15 Spectral diffusivity $K(\kappa)$ as a function of wavenumber κ. After Berkowicz and Prahm (1979).

When spectral diffusivity theory is used to predict the spread of smoke puffs within a homogeneous turbulent environment, the result shown in Fig 6.16 is a slow dispersion rate initially while the puff is small. Later, when the puff is larger, it grows at the same rate as would be expected for normal (nonspectral) K-theory. In the figure, $B_o = 0$ corresponds to the normal K-theory dispersion, while $B_o = 3\ m^{-4/3}$ is the dispersion with spectral diffusivity.

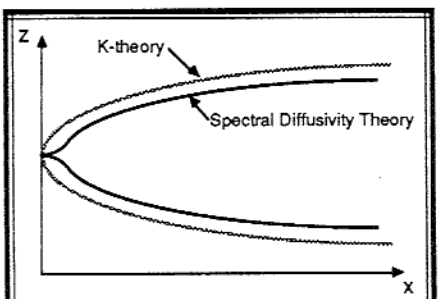

Fig. 6.16 Top and bottom edges of a passive tracer puff with downwind distance, for K-theory and spectral diffusivity theory. After Berkowicz and Prahm (1979).

The initial slower dispersion rate and non-Gaussian distribution of tracer concentration is common to both transilient theory and spectral diffusivity theory. Although some experimental evidence supports these results, they differ from those of statistical dispersion theory .

6.10 References

André, J.-C. & P. Lacarrere, 1985: Mean and turbulent structures of the oceanic surface layer as determined from one-dimensional third-order simulations. *J. Physical Ocean.*, **15**, 121-132.

André, J.-C., F. DeMoor, Pl. Lacerure, G. Therry, & R. DuVachat, 1978: Modeling the 24-hour evolution of the mean and turbulent structures of the planetary boundary layer. *J. Atmos. Sci.*, **35**, 1861-1883.

Beljaars, A.C.M., J.L. Walmsley, and P.A. Taylor, 1987: A mixed spectral finite-difference model for neutrally stratified boundary-layer flow over roughness changes and topography. *Bound.-Layer Meteor.*, **38**, 273-303.

Berkowicz, R., 1984: Spectral methods for atmospheric diffusion modeling. *Bound. Layer Meteor.*, **30**, 201-220.

Berkowicz, R. & L.P. Prahm, 1979: Generalization of K-theory for turbulent diffusion. Part 1: Spectral turbulent diffusivity concept. *J. Appl. Meteor.*, **18**, 266-272.

Bhumralkar, C.M., 1975: *A survey of Parameterization Techniques for the Planetary Boundary Layer in Atmospheric Circulation Models*. Defense Advanced Research Projects Agency R-1653-ARPA. ARPA order No. 189-1. 84pp.

Briere, S., 1987: Energetics of daytime sea-breeze circulation as determined from a two-dimensional, third-order turbulence closure model. *J. Atmos. Sci.*, **44**, 1455-1474.

Bougeault, P., 1981: Modeling the trade-wind cumulus boundary layer. Part 2: A high-order one-dimensional model. *J. Atmos. Sci.*, **38**, 2429-2439.

Bougeault, P., 1985: The diurnal cycle of the marine stratocumulus layer: A higher order

model study. *J. Atmos. Sci.*, **42**, 2826-2843.

Businger, J.A., 1982: Equations and concepts. *Atmospheric Turbulence and Air Pollution Modelling*, Edited by F.T.M. Nieuwstadt and H. van Dop, D. Reidel Publishing Co., Dordrecht., 1 - 36.

Chou, P.Y., 1945: On velocity correlations and the solutions of the equations of turbulent fluctuation. *Quart. J. Appl. Math.*, **3**, 38-54.

Deardorff, J.W., 1973: Three-dimensional numerical modeling of the planetary boundary layer.*Workshop on Micrometeorology*, Amer.Meteor.Soc., Ed: D.Haugen. 271-311.

Delage, Y., 1974: A numerical study of the nocturnal atmospheric boundary layer. *Quart. J. Roy. Meteor. Soc.*, **100**, 351-364.

Detering, H.W. and D. Etling, 1985: Application of the E-ε turbulence closure model to the atmospheric boundary layer. *Bound.-Layer Meteor.*, **33**, 113-133.

Donaldson, C. duP., 1973: Construction of a dynamic model of the production of atmospheric turbulence and the dispersal of atmospheric pollutants. *Workshop on Micrometeorology*, Edited by D.A. Haugen. American Meteorological Society, Boston. 313-392.

Ebert, E.E., U. Schumann, and R. B. Stull, 1989: Nonlocal turbulent mixing in the convective boundary layer evaluated from large-eddy simulation. *J. Atmos. Sci.*, **46**

Ekman, V.W., 1905: On the influence of the earth's rotation on ocean currents. *Arkiv. Math Astron. O. Fysik*, **2**, 11.

Estournel, C., and D. Guedalia, 1987: A new parameterization of eddy diffusivities for nocturnal boundary layer modeling. *Bound.-Layer Meteor.*, **39**, 191-203.

Haltiner, G.J. and R.T. Williams, 1980: *Numerical Prediction and Dynamic Meteorology*, 2nd ed. Wiley & Sons, 477pp.

Hanjalic, K. & B.E. Launder, 1972: A Reynolds' stress model of turbulence and its application to thin shear flows. *J. Fluid Mech.*, **52**, 609-638.

Keller, L.V. and A.A. Friedman, 1924: Differentialgleichung für die turbulente Bewegung einer Kompressiblen Flüssigkeit. *Proc. Ist Intern. Congr. Appl. Mech.*, Delft, 395-405.

Kitada, T., 1987: Turbulence transport of a sea breeze front and its implication in air pollution transport — application of k-ε turbulence model. *Bound. Layer Meteor.*, **41**, 217-239.

Lacser, A. and S.P.S. Arya, 1986: A comparitive assessment of mixing-length parameterizations in the stably stratified nocturnal boundary layer (NBL). *Bound.-Layer Meteor.*, **36**, 53-70.

Launder, B.E., G.J. Reece & W. Rodi, 1975: Progress in the development of a Reynolds-stress turbulence closure. *J. Fluid Mech.*, **68**, 537-566.

Lumley, J.L. & B. Khajeh-Nouri, 1974: Computational modeling of turbulent transport. *Adv. in Geophys.*, **18A**, Academic Press. 169-192.

Lumley, J.L. & P. Mansfield, 1984: Second-order modeling of turbulent transport in the surface mixed layer. *Bound.-Layer Meteor.*, **30**, 109-142.

Mellor, G.L. & J.R. Herring, 1973: *A.I.A.A. J.*, **11**, 590-599.

Mellor, G.L. & T. Yamada, 1974: A hierarchy of turbulence closure models for the planetary boundary layer. *J. Atmos. Sci.*, **31**, 1791-1806.

Moeng, C.-H. & D.A. Randall, 1984: Problems in simulating the stratocumulus-topped boundary layer with a third-order closure model. *J. Atmos. Sci.*, **41**, 1588-1600.

O'Brien, J.J., 1970: A note on the vertical structure of the eddy exchange coefficient in the planetary boundary layer. *J. Atmos. Sci.*, **27**, 1213-1215.

Pearson, C.E. (Ed.), 1974: *Handbook of Applied Mathematics, Selected Results and Methods*. Van Nostrand Reinhold Co., 1265pp.

Prahm, L.P.,R. Berkowicz & O. Christensen, 1979: Generalization of K-theory for turbulent diffusion. Part 2: Spectral diffusivity model for plume dispersion. *J. Appl. Meteor.*, **18**, 273-282.

Prandtl, L., 1910: Bericht über Untersuchungen zur ausgebildeten Turbulenz. *Zs. angew. Math. Mech.*, **5**, 136-139.

Ray, D., 1986: Variable eddy diffusivities and atmospheric cellular convection. *Bound.-Layer Meteor.*, **36**, 117-131.

Rotta, J.C., 1951: Statistische theorie nichthomogener turbulenz. *Zeitschrift für Phys.*, **129**, 547-572.

Schumann, U. 1977: Realizability of Reynolds' stress turbulence models. *Phys. Fluids*, **20**, 721-725.

Stull, R.B., 1984: Transilient turbulence theory. Part 1: The concept of eddy mixing across finite distances. *J. Atmos. Sci.*, **41**, 3351-3367.

Stull, R.B., 1986: Transilient turbulence theory. Part 3: Bulk dispersion rate and numerical stability. *J. Atmos. Sci.*, **43**, 50-57.

Stull, R.B., 1987: Transilient turbulence algorithms to model mixing across finite distances. *Environmental Software*, **2**, 4-12.

Stull, R.B. and A.G.M. Driedonks, 1987: Applications of the transilient turbulence parameterization to atmospheric boundary-layer simulations. *Bound.-Layer Meteor.*, **40**, 209-239.

Sun, W-H. and Y.Ogura, 1980: Modeling the evolution of the convective planetary boundary layer. *J. Atmos. Sci.*, **37**, 1558-1572.

Wai, M.M.-K., 1987: A numerical study of the marine stratocumulus cloud layer. *Bound.-Layer Meteor.*, **40**, 241-267.

Wichmann, M. and E. Schaller, 1985: Comments on "Problems in simulating the stratocumulus-topped boundary layer with a third-order closure model". *J. Atmos. Sci.*, **42**, 1559-1561.

Wichmann, M. and E. Schaller, 1986: On the determination of the closure parameters in higher-order closure models. *Bound.-Layer Meteor.*, **37**, 323-341.

Wyngaard, J.C., O.R. Coté, K.S. Rao, 1974: Modeling of the atmospheric boundary layer. *Adv. in Geophys.*, **18A**, Academic Press, 193-212.

Wyngaard, J.C., 1982: Boundary layer modeling. *Atmospheric Turbulence and Air Pollution Modelling*, Edited by F.T.M. Nieuwstadt and H. van Dop, D. Reidel Publ. Co., Dordrecht, 69-106.

Yamada, T. & G. Mellor, 1975: A simulation of the Wangara atmospheric boundary layer data. *J. Atmos. Sci.*, **32**, 2309-2329.

Zeman, O., 1981: Progress in the modeling of planetary boundary layers. *Ann. Rev. Fluid Mech.*, **13**, 253-272.

6.11 Exercises

1) Which turbulence closure scheme would be most appropriate for the atmospheric boundary layers in each of the following applications? Why?
   a) Nested Grid Model (NGM) numerical forecast model (or other operational weather forecast model).
   b) Diffusion of smoke from a tall stack.
   c) Mesoscale numerical forecast model for the interior of continents.
   d) Sea-breeze numerical forecast model for your favorite coastline.
   e) Air flow through the turbine disks in a jet engine.
   f) 3-D numerical thunderstorm model.
   g) Global climate model
   h) Numerical model of individual thermals in the BL.
   i) Study of the air flow over complex terrain for wind energy siting.
   j) Study of heat, moisture, and mass transfer over a ginseng crop.
   k) Forecasting minimum daily temperatures at your town.
   l) Study the moisture budget of a hurricane.
   m) Study the turbulence structure of the Venusian atmosphere.
   n) Forecasting the nocturnal jet.
   o) Numerical simulation of the interaction between ocean currents and the atmosphere.
2) Very briefly define the following, and comment or give examples of their use in micrometeorology:
   a) Ekman spiral
   b) Turbulence closure problem
   c) K-theory
3) Write a correlation triangle for third-order closure similar to the lower-order triangles in Table 6-2.
4) What is the closure problem, and how does it affect the study of turbulent boundary layers?
5) Given:

z	12	8	2	$0.1=z_o$	(m)
$\overline{\theta}$	300	301	303	308	(K)
$\overline{U}$	5.4	5.0	3.4	0	(m/s)

   Use first-order closure to find $\overline{w'\theta'}$ and $\overline{u'w'}$ at $z = z_o$ and at $z = 10$ m.
6) What advantages and disadvantages are there for using one-and-a-half-order closure, as compared to first-order closure?
7) Use K-theory to find the heat flux as a function of height, given a potential temperature profile of the shape $\theta = \theta_o - a \ln(z/z_o)$, where $\theta_o = 300$ K at $z = z_o = 1$ mm, and $a = 5$ K. Assume that $K = k z u_*$ with $u_* = 0.1$ m/s and $k=0.4$.

8) What order closure (zero, first, 1 1/2, second, third) is used in the derivation of the Ekman spiral?

9) Can transilient turbulence closure simulate K-theory diffusion? Can K-theory simulate looping smoke plumes?

10) For an eddy diffusivity of $K_m = 2\ m^2 s^{-1}$ and a geostrophic vorticity of $0.0001\ s^{-1}$ with an average tangential velocity of 8 m/s, calculate the vertical velocity at Madison, Wisconsin caused by "Ekman pumping" at the top of a 500 m thick boundary layer.

11) What is a common first-order closure method?

12) Given the following matrix of transilient coefficients:

$$c_{ij}\ (\Delta t = 10\ \text{min}) = \begin{bmatrix} 0.1 & 0.9 & 0. & 0. & 0. \\ 0.2 & 0.05 & 0.75 & 0. & 0. \\ 0.25 & 0.05 & 0.2 & 0.5 & 0. \\ 0.25 & 0. & 0.05 & 0.3 & 0.4 \\ 0.2 & 0. & 0. & 0.2 & 0.6 \end{bmatrix}$$

a) Verify that mass and state are conserved, and that entropy increases.

b) Given an initial state of pollution concentration in the boundary layer of

Grid index (i)	z (m)	S (g/m^3)
1	100	500
2	300	0
3	500	0
4	700	0
5	900	0

Forecast the pollution concentration at each of these heights every 10 min from t=0 to t=90 min. (Assume a 1km thick boundary layer, with 5 grid points centered at the heights indicated above, with $\Delta z = 200$ m.)

c) Plot a time height diagram of your results from (b), and draw isopleths for S = 90, 110, and 130 g/m^3. Comment on the behavior of the pollutants, and on what type of boundary layer (ML, NBL, RL) is probably there.

d) Find and plot the flux profile associated with the first and second timesteps.

e) If a timestep of Δt=30 min were desired instead, calculate the new matrix of transilient coefficients.

f) Using the answer from (b), make a new forecast of pollutant concentration from t=0 to t=90 min, using Δt=30 min and the same initial conditions as before. Compare your answer to that of part (b).

g) If the rows of the transilient coefficient matrix given at the top of this page were switched, such that the bottom row is at the top, the second to the bottom becomes second from the top, etc., then comment on the nature of smoke dispersion.

13) Given the following transilient coefficient matrix

$$c_{ij}\ (\Delta t = 10\ \text{min}) = \begin{bmatrix} 0.7 & 0.2 & 0.1 & 0.0 \\ 0.2 & 0.7 & 0.2 & 0.1 \\ 0.1 & 0.2 & 0.7 & 0.2 \\ 0.0 & 0.1 & 0.2 & 0.7 \end{bmatrix}$$

a) What is wrong with this matrix?

b) Make a forecast (only out to t=10 min) to demonstrate your conclusions from part (a). Start with an initial tracer concentration distribution given by

index	concentration
1	0
2	0
3	100
4	0

14) Let $K_m = 5\ m^2 s^{-1}$ = constant with height. Calculate and plot

a) $\overline{u'w'}$ b) $\overline{w'\theta_v'}$

from z=0 to 50 m using the data from problem 26 of Chapt. 5.

15) a) Using the answers from problem (14) above, find the initial tendency for virtual potential temperature $(\partial\overline{\theta_v}/\partial t)$ for air at a height of z=10 m.

b) If this tendency does not change with time, what is the new $\overline{\theta_v}$ at z=10 m, one hour after the initial state (i.e., the state of problem 26, Chapt. 5)?

16) Verify the Ekman boundary layer solutions by plugging them back into the original differential equations, and by checking to see if they satisfy the boundary conditions.

17) Given $K_m = k\ z\ u_*$. Solve for $\overline{U}$ as a function of height in the SL.

18) For 1.5-order closure, indicate which prognostic equations are needed to forecast $\overline{\theta'^2}$? To save time, write only the storage term for each equation used. Hint, one of the equations is $\partial\,\overline{\theta'^2}/\partial t = \ldots$

19) Given the following matrix of transilient coefficients:

$$c_{ij}\ (\Delta t = 30\ \text{min}) = \begin{bmatrix} 0.3 & 0.25 & 0.25 & 0.2 \\ 0.25 & 0.3 & 0.25 & 0.2 \\ 0.25 & 0.25 & 0.3 & 0.2 \\ 0.2 & 0.2 & 0.2 & 0.4 \end{bmatrix} \quad \begin{matrix} \text{index} \\ 1 \\ 2 \\ 3 \\ 4 \end{matrix}$$

a) Does this matrix satisfy mass and state conservation? Why?

b) Describe the nature of mixing (e.g., overturning, small-eddies, no turbulence, well mixed, sub-domain of turbulence, etc.)

c) Given the following initial concentrations, find the new concentrations after 30 min.

index	concentration
1	100
2	100
3	200
4	0

d) Find the flux profile for this one timestep, given $\Delta z = 100$ m.

20) Given the following transilient matrix:

$$c_{ij}\ (\Delta t = 10\ \text{min}) = \begin{bmatrix} 0.7 & 0.2 & 0.1 & 0. & 0. & 0 \\ 0.2 & 0.5 & 0.2 & 0.1 & 0. & 0 \\ 0.1 & 0.2 & 0.4 & 0.2 & 0.1 & 0 \\ 0. & 0.1 & 0.2 & ? & 0.2 & 0 \\ ? & ? & ? & ? & ? & ? \\ 0 & 0 & 0 & 0 & 0 & 1 \end{bmatrix}$$

a) Fill in the missing elements.

b) In the interior of the turbulent domain, is the turbulence homogeneous? Is it isotropic (in one dimension)?

c) Comment on the kind of turbulent boundary layer parameterized by the matrix above? (That is, what is the nature of the turbulence: diffusive, convective, other...)

d) Given the following initial distribution of pollutant concentration (S, in units of micrograms per cubic meter) at each of six grid points, forecast the concentration at t=10, 20, & 30 minutes using a Δt=10 min timestep.

Grid Index	z (m)	S
1	50	100
2	150	0
3	250	0
4	350	0
5	450	0
6	550	0

Check to be sure that pollutant mass is conserved at each time.

e) Find the flux as a function of height for the first timestep.

f) Comment on the centroid of pollutant concentration, and how it moves with time.

g) After 100 timesteps, qualitatively discuss the anticipated vertical distribution of pollutants. (i.e., you need not make an actual forecast).

21) Given the following transilient matrix:

$$c_{ij}\ (\Delta t = 15\ \text{min}) = \begin{bmatrix} 0.7 & 0 & 0.2 & 0.1 \\ 0.1 & 0.6 & ? & 0.2 \\ ? & ? & ? & ? \\ 0.1 & 0.2 & ? & 0.3 \end{bmatrix}$$

a) Fill in the missing elements to yield an allowable matrix.

b) Given an initial tracer distribution of 100 mg m^{-3} at the lowest grid box (i=1), 10 mg m^{-3} in the top grid box (i=4), and no tracer elsewhere, find the tracer distribution after 15 minutes.

c) Was tracer amount conserved? How do you know?

d) Does the transilient matrix represent homogeneous turbulence?

e) Does the transilient matrix represent isotropic turbulence?

22) If one considers only the momentum equations, how many total equations and unknowns (only of velocity correlations in this case) are there for fourth-order closure? (Hint, look at Table 6-1.)

23) Given an initial pollutant concentration distribution of

index	z(m)	concentration
1	10	0
2	30	0
3	50	0
4	70	100
5	90	0

and a transilient matrix of:

$$c_{ij}\ (\Delta t = 5\ \text{min}) = \begin{bmatrix} 0.6 & 0.4 & 0 & 0 & 0 \\ 0.4 & 0.3 & 0.3 & 0 & 0 \\ 0 & 0.3 & 0.6 & 0.1 & 0 \\ 0 & 0 & 0.1 & 0.9 & 0 \\ 0 & 0 & 0 & 0 & 1 \end{bmatrix}$$

a) Find the new concentrations S_i at $t = 10$ min.

b) When would pollutants first reach the lowest grid box?

c) Is there a way to find the concentrations at $t = 10$ min in just one timestep, starting from the concentration at $t = 0$?

d) Find and plot the flux profile.

24) Does the following closure method obey the rules of parameterization?

a) The first-order closure of equation (6.4.1b).

b) The one-and-a-half-order closure of equation (6.5b) for heat flux.

c) The second-order parameterizations by Deardorff for $\overline{\theta' u_i' u_j'}$ (see Table 6-5).

d) The second-order parameterization by Rotta for the pressure correlation (see Table 6-5).

25) Without using the assumption that the mixing length is proportional to height above the ground, rederive the mixing-length expression for moisture flux for the case where a solid boundary limits the maximum size of eddies. Hint, use a statistical approach with a probability distribution that is zero beyond the solid boundary.

26) Given the heat flux profiles in Figs 3.1, 3.2, and 3.3, and the mean profiles of potential temperature in Figs. 3.4 and 3.5:

a) calculate the value for K_H as a function of height for :

(1) Flight 2
(2) Flight 3
(3) Flight 13

b) Which parameterization in Table 6-4 best fits the calculated K values from part (a)?

27) For an eddy viscosity of 10 $m^2 s^{-1}$, and a pressure gradient of 0.2 kPa / 100 km in the atmosphere, plot the Ekman spiral winds as a function of height, and find the Ekman layer depth at:

a) Bergen, Norway

b) Madison, Wisconsin

c) Christmas Island (in the Line Islands)

28) Suggest a parameterization for $\overline{u_i' u_j' u_k' u_m'}$.

29) Given the γ_T and θ curves in the following figure, calculate the initial tendency (TM) due to turbulent mixing using the continuous form of transilient turbulence theory.

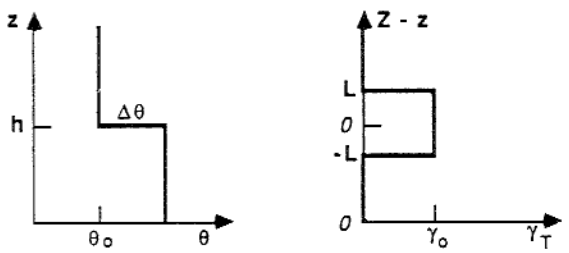

30) Use spectral diffusivity theory to solve problem (29), using $K_o = 2\ m^2 s^{-1}$ and $B_o = 3$. (i.e., do not use γ_T for this case). Also, plot K vs. κ.

31) Given the following heat flux and potential temperature gradients, find and plot K_H vs z/z_i . Comment on the meaning of K_H at each height.

z/z_i	$\overline{w'\theta'}$ (K m/s)	$\partial\bar{\theta}/\partial z$ (K/m)
0.0	0.20	-0.020
0.2	0.15	-0.005
0.4	0.10	-0.001
0.6	0.05	0.001
0.8	0.00	0.005
1.0	-0.05	0.020